Article

A skeletal muscle–sympathetic nerve–intestine network underlies muscle inflammation and atrophy induced by immobilization

Yu Hirata,[1] Kazuhiro Nomura,[1,2] Kaori Hozumi,[1] Kenji Sugawara,[1] Yusei Hosokawa,[1] Kana Uchiyama,[1] Tomoya Inoue,[1] Tomoko Nishigaki,[1] An Liyuan,[1] Takahiro Niikura,[3,4] Tomoaki Fukui,[3] Keisuke Oe,[3] Ryosuke Kuroda,[3] Sotaro Hamakita,[5] Shohei Kumagai,[6] Jun Hirata,[6] Gerard Karsenty,[7] Kento Ohbayashi,[8] Toshihiko Yada,[9,10,11] Yusaku Iwasaki,[8] and Wataru Ogawa[1,12,*]

[1]Division of Diabetes and Endocrinology, Department of Internal Medicine, Kobe University Graduate School of Medicine, Kobe, Japan
[2]Department of Nutrition and Metabolism, Institute of Biomedical Sciences, Tokushima University Graduate School, Tokushima, Japan
[3]Department of Orthopaedic Surgery, Kobe University Graduate School of Medicine, Kobe, Japan
[4]Department of Orthopaedic Surgery, Hyogo Prefectural Nishinomiya Hospital, Hyogo, Japan
[5]R&D, Noster Inc., Kyoto, Japan
[6]Pharmaceutical Discovery Research Laboratories, Teijin Pharma Limited, Hino, Japan
[7]Department of Genetics and Development, Vagelos College of Physicians and Surgeons, Columbia University, New York, NY, USA
[8]Laboratory of Animal Science, Graduate School of Life and Environmental Sciences, Kyoto Prefectural University, Kyoto, Japan
[9]Center for Integrative Physiology, Kansai Electric Power Medical Research Institute, Kyoto, Japan
[10]Department of Diabetes, Endocrinology and Metabolism/Rheumatology and Clinical Immunology, Gifu University Graduate School of Medicine, Gifu, Japan
[11]Division of Diabetes, Metabolism and Endocrinology, Kobe University Graduate School of Medicine, Kobe, Japan
[12]Lead contact
*Correspondence: ogawa@med.kobe-u.ac.jp

SUMMARY

Immobility is a common cause of muscle atrophy, but the underlying mechanisms have remained unclear. Here we show that limb immobilization in mice elicits inflammation and atrophy of skeletal muscle that are preventable by neutralizing antibodies to the chemokine CXCL10. Limb immobilization also induced changes to the gut microbiota and intestinal inflammation, and either sterilization of the intestine with antibiotics or administration of 10-hydroxy-*cis*-12-octadecenoic acid—a linoleic acid–derived gut microbial metabolite—prevented intestinal and muscle inflammation as well as muscle atrophy induced by immobilization, implicating intestinal inflammation in muscle inflammation and atrophy. Limb immobilization activated sympathetic nerves and increased β2-adrenergic receptor gene (*Adrb2*) expression in the intestine. Single-cell RNA-sequencing analysis revealed that, among cells expressing *Adrb2* in the intestine, immobilization increased only the population of macrophages. Pharmacological inhibition or macrophage-specific ablation of Adrb2 prevented immobilization-induced intestinal and muscle inflammation. Our results thus implicate a previously unrecognized muscle-nerve-intestine network in immobilization-induced muscle atrophy.

KEYWORDS

Muscle atrophy, immobility, inflammation, CXCL10, gut microbiota, β2-adrenergic receptor, gut microbial metabolite, 10-hydroxy-*cis*-12-octadecenoic acid, single-cell RNA sequencing

INTRODUCTION

Muscle mass is an important determinant of human health. A reduction in muscle mass together with the consequent decline in physical performance can trigger or accelerate various pathological conditions.[1] Exercise is an important stimulus for muscle growth,[2] and immobilization is one of the most common causes of muscle mass loss.[3] The decline in muscle mass induced by immobilization is attributable at least in part to the loss of exercise stimulation.[4] However, whereas the exercise-induced increase in muscle mass generally occurs over a time span of weeks to months, immobilization elicits a more rapid decline in muscle mass, sometimes within just a few days,[5] suggesting that immobilization actively triggers mechanisms that reduce muscle mass in a manner independent of the loss of exercise-induced muscle growth. The mechanisms by which immobilization proactively induces muscle mass loss have remained unclear, however.

We recently showed that limb immobilization, either by cast-fixation or motor nerve resection, results in a decline in the basal intracellular Ca^{2+} concentration of muscle cells through downregulation of the Ca^{2+} channel Piezo1.[6] This reduction in the cytosolic Ca^{2+} level in turn promotes protein catabolism in a manner dependent on the transcription factor KLF15 and the cytokine interleukin (IL)–6. These findings suggest that an increase in protein catabolism mediated by a Piezo1/KLF15/IL-6 pathway is a key contributor to the loss of muscle mass actively triggered by immobility.[6] On the other hand, inflammatory signals have also been implicated in immobility-induced muscle atrophy,[7,8] although the relation between protein catabolism and inflammation during immobility has remained unclear.

To provide further insight into the mechanisms by which immobility induces muscle atrophy, we have now investigated the time-dependent changes in skeletal muscle during limb immobilization. We found that the prominent pathological effect of limb immobilization on skeletal muscle transitions from protein catabolism to inflammation in a time-dependent manner. We also found that this muscle inflammation is dependent on changes to the gut microbiota and on intestinal inflammation triggered by the activation of sympathetic nerves in the intestine.

RESULTS

Transition from protein catabolism to inflammation during skeletal muscle immobilization

We previously showed that limb immobilization for a relative short period (up to 3 days) induced by either cast-fixation or motor nerve resection results in a decline in skeletal muscle mass through an increase in protein catabolism mediated by a

Piezo1/KLF15/IL-6 axis.[6] We here investigated how more prolonged limb immobilization affects skeletal muscle. Cast-fixation of the hind limbs of mice resulted in a significant reduction in muscle mass of the immobilized limbs within the first 3 days of immobilization, and this decline in muscle mass continued thereafter in a time-dependent manner (Figure 1A). The progression of muscle fiber atrophy during immobilization was confirmed by a decrease in muscle fiber area detected by histological analysis (Figures 1B and 1C). Immunohistochemical staining revealed that limb immobilization for 10 days, but not that for 3 days, resulted in a significant accumulation of cells positive for the macrophage marker F4/80 in the affected muscle (Figures 1B and 1D). Flow cytometry also revealed an increase in the proportion of $CD11b^{+}F4/80^{+}$ cells among $CD45^{+}Ly6G^{-}$ cells in muscle (Figures 1E and 1F), and that the percentages of $CD11c^{+}CD206^{-}$ and $CD11c^{-}CD206^{+}$ cells among these $CD11b^{+}F4/80^{+}$ cells were increased and decreased, respectively, after limb immobilization for 10 days (Figures S1A–S1C). These results thus indicated that limb immobilization for 10 days induced the accumulation of macrophages in skeletal muscle as well as increased and decreased the proportions of pro-inflammatory and anti-inflammatory subsets of these cells, respectively.

Reverse transcription and quantitative polymerase chain reaction (RT-qPCR) analysis revealed that the expression of genes related to protein catabolism was upregulated in immobilized muscle, peaking at 1 to 3 days (Figure 1G), consistent with our previous findings.[6] In contrast, the expression of genes related to inflammation was significantly upregulated during a later phase of immobilization, peaking at 10 days (Figure 1G). RNA–sequencing (seq) analysis of immobilized muscle indicated that genes related to the proteasome, protein processing in the endoplasmic reticulum (ER), mitophagy, and autophagy were upregulated at 3 days (Figure 1H), whereas those related to cytokine–cytokine receptor interaction, hematopoietic cell lineage, phagosome, and chemokine signaling pathway were upregulated after immobilization for 10 days (Figure 1I). Gene set enrichment analysis (GSEA) also confirmed the upregulation of genes related to the proteasome or to cytokine–cytokine receptor interaction after 3 and 10 days of immobilization, respectively (Figures S1D and S1E).

Hind limb immobilization induced by motor nerve denervation similarly resulted in a time-dependent decline in skeletal muscle mass that was associated with the upregulation of genes related to protein catabolism or to inflammation at 3 and 10 days, respectively, as well as with the accumulation of F4/80-positive cells at 10 days (Figure S2). Together, these results thus revealed a transition from protein catabolism to inflammation during muscle atrophy triggered by prolonged limb immobilization.

CXCL10 mediates inflammation and atrophy of muscle induced by immobilization

We next attempted to identify a humoral factor that might contribute to muscle inflammation during limb immobilization. RNA-seq analysis indicated that the gene for the chemokine CXCL10 was one of the most markedly induced inflammatory humoral factor genes in skeletal muscle under this condition (Figures 2A and 2B). The expression of *Cxcl10* was increased 1 day after the onset of limb immobilization by cast-fixation, peaked at 7 days, and decreased thereafter (Figure 2C). The circulating concentration of CXCL10 was similarly increased during limb immobilization (Figure 2D). The upregulation of *Cxcl10* expression was apparent in both the blood cell and non–blood cell fractions of muscle, which were discriminated on the basis of the expression of CD45 (Figure S3A); however, it was more pronounced in the non–blood cell fraction, which was composed mostly of myofibers. A similar increase in *Cxcl10* expression was also detected in skeletal muscle of denervated mice (Figure 3SB). Of note, upregulation of the CXCL10 gene (Figure 2E) and of other inflammation-related genes (Figure S3C) was observed in human skeletal muscle after cast-fixation for an average of 8.3 ± 3.1 days as a result of bone fractures. Furthermore, analysis of publicly available human gene expression data revealed that acute immobilization of lower limbs was associated with an increase in the abundance of *CXCL10* mRNA in skeletal muscle (Figure S3D).

The administration of neutralizing antibodies to CXCL10 inhibited both the accumulation of macrophages (Figures 2F and 2G) and the upregulation of inflammation-related gene expression (Figure 2H) in muscle during subsequent limb immobilization by cast-fixation. These antibodies also attenuated the decrease in both skeletal muscle mass (Figure 2I) and muscle fiber area (Figures 2F and 2J) induced by prolonged limb immobilization. In contrast, the neutralizing antibodies to CXCL10 did not affect the upregulation of catabolism-related genes or the decline in muscle mass apparent after limb immobilization for 3 days (Figures S3E and S3F). Collectively, these findings suggested that inflammation mediated by CXCL10 plays a key role in the loss of muscle mass induced by immobilization, whereas protein catabolism, which is activated relatively early during immobilization, is independent of this CXCL10 pathway.

Prolonged limb immobilization induces inflammation in the intestine

Given that prolonged limb immobilization gives rise to inflammation in skeletal muscle, we next explored whether such immobilization also induces inflammation in other

organs. Examination of the entire body of cast-immobilized mice revealed intestinal shortening (Figures 3A and 3B), a decrease in cecum mass (Figure 3C), and a reduction in the depth of crypts in the colon (Figures 3D and 3E), all of which are associated with intestinal inflammation.[9] A decrease in tissue mass was also apparent for the small and large intestine, but not for the stomach or duodenum (Figure S4A). The reduction in the length of the small and large intestine as well as that in cecum mass became evident within 7 to 10 days of the onset of limb immobilization (Figures S4B and S4C), showing a time course similar to that of skeletal muscle inflammation. Immunohistochemical analysis and flow cytometry revealed that prolonged limb immobilization resulted in the accumulation of F4/80-positive cells and $CD11b^{+}F4/80^{+}$ cells, respectively, in the intestinal wall (Figures 3D and F–H), with a concomitant increase in the proportion of pro-inflammatory ($CD11c^{+}CD206^{-}$) and decrease in that of anti-inflammatory ($CD11c^{-}CD206^{+}$) macrophages (Figures S4D–S4F). In addition, RT-qPCR analysis showed that the expression of inflammation-related genes was upregulated in the distal small intestine and colon, but not in the proximal small intestine, of mice subjected to cast-fixation for 10 days (Figure S5A). GSEA of RNA-seq data obtained from the intestine of such mice revealed upregulation of genes related to inflammation, including those associated with cytokine and chemokine signaling pathways (Figure 3I). Denervation-induced limb immobilization for 10 days also resulted in intestinal shortening (Figure S5B), a decrease in cecum mass (Figure S5C), and upregulation of inflammation-related genes in the distal small intestine and colon (Figure S5D).

Intestinal inflammation is typically associated with impairment of the intestinal barrier, resulting in an increase in the circulating levels of bacterial components such as lipopolysaccharide (LPS).[10] Consistent with this scenario, prolonged limb immobilization resulted in a decrease in the intestinal abundance of claudin-1 (Figure 3J), a key protein in maintenance of the intestinal barrier,[11] and in an increase in the plasma concentration of LPS (Figure 3K). Furthermore, treatment of cultured C2C12 myotubes with LPS resulted in the upregulation of *Cxcl10* expression (Figure 3L). Collectively, these results suggested that prolonged limb immobilization triggers intestinal inflammation, which may then contribute to upregulation of CXCL10 expression and consequent induction of inflammation in skeletal muscle.

The gut microbiota contributes to inflammation and atrophy of skeletal muscle induced by limb immobilization

The development of intestinal inflammation is closely related to changes in the gut microbiota.[10] We therefore investigated the impact of prolonged limb immobilization on the gut microbiota. Analysis of bacterial 16S rRNA genes revealed that prolonged immobilization of the hind limbs of mice by cast-fixation resulted in marked changes to the gut microbiota including an increase in the abundance of the Lachnospiraceae group and a decrease in that of *Lactobacillus* species (Figures 4A and 4B). These changes in the gut microbiota were also demonstrated by principal component analysis (Figure 4C), and they were largely reversed within 2 weeks after cast removal (Figures S6A–S6C), indicating that the changes were indeed primarily triggered by limb immobilization. Furthermore, limb immobilization by motor nerve denervation resulted in changes to the gut microbiota similar to those induced by cast-fixation (Figures S6D and S6E). Pseudosterilization of the intestine by oral administration of antibiotics attenuated the inflammation of skeletal muscle and the decline in muscle mass induced by cast-fixation of hind limbs (Figures 4D and 4E). These results thus implicated the gut microbiota in the inflammation and atrophy of skeletal muscle triggered by prolonged limb immobilization.

A gut microbial metabolite derived from linoleic acid inhibits intestinal and muscle inflammation as well as muscle atrophy induced by limb immobilization

We next examined whether the prevention of intestinal inflammation might ameliorate the loss of skeletal muscle induced by prolonged limb immobilization. We focused on gut microbial metabolites derived from linoleic acid (LA), which have been shown to exert various biological effects including the prevention of drug-induced colitis.[12-14] Analysis of various LA-derived fatty acid metabolites (Figure S7A) in feces by mass spectrometry revealed that limb immobilization by cast-fixation for 10 days reduced the abundance of LA and 13-hydroxy-*cis*-9-octadecenoic acid (HYD) and that limb denervation for 10 days reduced that of HYD and 10-hydroxy-*cis*-12-octadecenoic acid (HYA) as well as that of metabolites derived from these two fatty acids including 13-oxo-*cis*-9-octadecenoic acid (KetoD), 10,13-dihydroxy-octadecanoic acid (HYE), 10-oxo-*cis*-12-octadecenoic acid (KetoA), and 10-oxo-*trans*-11-octadecenoic acid (KetoC) (Figures S7B and S8A), indicating that limb immobilization altered LA metabolism in the intestine.

Given that the abundance of LA, together with that of HYA and HYD, both of which are directly derived from LA, was decreased during limb immobilization, we fed mice with normal chow or chow containing these fatty acids for 10 days and then subjected them to limb immobilization. Dietary supplementation with LA or either of

the LA metabolites did not influence chow intake (Figure S8B). Oral administration of HYA, but not that of LA or HYD, attenuated the reduction in crypt depth and the accumulation of F4/80-positive cells in the colon (Figures 5A–5C) as well as the shortening of the colon (Figure S9A) induced by cast-fixation. Furthermore, treatment with HYA inhibited the upregulation of inflammation-related gene expression (Figure S9B) and the downregulation of claudin-1 protein (Figure S9C) in the colon triggered by prolonged limb immobilization. Gene ontology (GO) analysis of RNA-seq data for the colon revealed that the top 20 processes enriched among genes whose expression was upregulated by immobilization include various inflammatory cell–related categories (Figure S10A) and that treatment of limb-immobilized mice with HYA attenuated the expression of genes in these categories (Figure S10B). In addition, HYA, but not LA or HYD, prevented the immobilization-induced increase in the plasma concentration of LPS (Figure S10C).

Oral administration of HYA, but not that of LA or HYD, also attenuated the decline in muscle mass (Figure 5D) as well as the reduction in muscle fiber area and the accumulation of F4/80-positive cells in soleus muscle (Figures 5E and S11A and S11B) induced by limb immobilization. Furthermore, HYA treatment suppressed the immobilization-induced upregulation of inflammation-related gene expression in skeletal muscle (Figure S11C). Together, these data indicated that oral administration of HYA ameliorated intestinal inflammation, which in turn resulted in attenuation of inflammation and atrophy of skeletal muscle, in mice subjected to limb immobilization.

Sympathetic nerve activation contributes to intestinal inflammation induced by limb immobilization

We next investigated the mechanism by which limb immobilization triggers intestinal inflammation. We examined the possible role of the nervous system—in particular, the sympathetic nervous system—given that sympathetic nerves regulate immune responses in various tissues including the intestine.[15,16]

We first assessed sympathetic nerve activity by measuring the turnover of norepinephrine (NE) as previously described.[17,18] The NE content of tissue was thus determined before and after the intraperitoneal administration of α-methyl-*p*-tyrosine (α-MT), an inhibitor of catecholamine synthesis. As expected, α-MT treatment reduced NE content in all parts of the digestive tract examined (Figure 6A). Whereas the extent of the decrease in NE content induced by α-MT was similar for the stomach and the duodenum between control mice and mice subjected to cast-immobilization for 10 days, that for the proximal or distal small intestine or for the colon was greater in immobilized

mice (Figures 6A and 6B), indicating that NE turnover, which reflects sympathetic nerve activity, was selectively augmented in the lower intestine of the immobilized animals.

RNA-seq analysis of the colon revealed that, among genes encoding adrenergic receptors, the gene for the β2-adrenergic receptor (*Adrb2*) was most markedly upregulated by limb immobilization, and this upregulation was attenuated by dietary intake of HYA (Figure 6C). Expression of the gene for the α2a-adrenergic receptor (*Adra2a*) showed a similar pattern of changes, albeit to a lesser extent compared with the changes apparent for *Adrb2* expression. Treatment of mice with α-MT or the β2-adrenergic receptor antagonist propranolol, but not that with the α-adrenergic receptor antagonist phentolamine, inhibited the upregulation of inflammation-related genes in the intestine (Figure 6D) and skeletal muscle (Figure S12A). These results suggested that sympathetic nerve activation contributes to immobilization-induced inflammation of the intestine and skeletal muscle via the activation of Adrb2. Treatment with propranolol or α-MT did not affect immobilization-induced muscle atrophy, however (Figure S12B). Given that Adrb2 in myofibers plays an important role in muscle hypertrophy,[19,20] an antiatrophic effect of these inhibitors mediated by attenuation of Adrb2 signaling in the intestine might have been counteracted by an antihypertrophic effect mediated by attenuation of Adrb2 signaling in muscle.

To identify cell types that mediate Adrb2 signaling in the intestine, we performed single-cell (sc) RNA-seq analysis of the colon. The single-cell fixed RNA profiling method[21] allowed us to concomitantly analyze various cell types—including epithelial, stromal, and immune cells—while maintaining their transcriptional characteristics, leading to the identification of 37 cell clusters (Figures 6E and S12C). Genes that characterize each cell cluster are listed in Table S1. Cast-immobilization of hind limbs for 10 days increased the population size for various immune cell clusters including all four macrophage clusters, a macrophage/dendritic cell cluster, a dendritic cell cluster, a B cell/IgA plasma cell cluster, an IgA plasma cell cluster, and one of the two T cell clusters (Figure 6F).

Adrb2 mRNA was most abundant in two of the macrophage clusters (Macrophage_1 and Macrophage_2), one of the two B cell clusters (B cell_2), and a lymphatic endothelial cell cluster (Figures 6G and S13). Among these cell types, only the population of macrophages was increased in response to limb immobilization (Figure 6F). We therefore focused on this cell type and generated macrophage-specific Adrb2 knockout (Mφ-Adrb2KO) mice. The immobilization-induced increase in population size was attenuated for three of the four macrophages clusters

(Macrophage_2, _3, and _4), which express *Itgam* (Cd11b), *Fcer1g*, or *Cd14* and therefore likely correspond to pro-inflammatory macrophages, in Mφ-Adrb2KO mice (Figure 7A and Table S1). In contrast, *Adrb2* ablation increased the population size for the Macrophage_1 cluster, which expresses the anti-inflammatory macrophage markers *Cd163* and *Mrc1*,[22] in the colon of mice subjected to limb immobilization (Figure 7A and Table S1). Consistent with these findings, flow cytometry revealed that the limb immobilization–induced increase in the abundance of pro-inflammatory macrophages in the colon was prevented in Mφ-Adrb2KO mice (Figures 7B and 7C as well as S14A and S14B). Moreover, the reduction in crypt depth and the accumulation of F4/80-positive cells (Figures 7D–7F) as well as the upregulation of *Ccl2* expression (Figure S14C) in the colon induced by limb immobilization were also all attenuated in Mφ-Adrb2KO mice.

The accumulation of macrophages and the increase in the proportion of pro-inflammatory macrophages in skeletal muscle induced by prolonged limb immobilization were also inhibited, whereas the decrease in the proportion of anti-inflammatory macrophages was unaffected, in Mφ-Adrb2KO mice (Figures 7G as well as S14E and S14F). The decline in skeletal muscle mass induced by immobilization tended to be attenuated in Mφ-Adrb2KO mice, although this effect was not statistically significant (Figure 7H). Collectively, these results suggested that Adrb2 signaling in intestinal macrophages plays a key role in skeletal muscle inflammation induced by limb immobilization.

DISCUSSION

We have here shown that the pathology of skeletal muscle associated with limb immobilization transitions from catabolism to inflammation, with the latter process being regulated by CXCL10 (Figure 7I). Limb immobilization results in changes to the gut microbiota and intestinal inflammation that subsequently contribute to the development of muscle inflammation. Furthermore, the onset of intestinal inflammation is triggered by sympathetic nerve activation and Adrb2 signaling in macrophages. Our results have thus uncovered a muscle-neural-intestinal network that underlies the development of muscle atrophy in response to limb immobilization.

Whereas changes to the intestinal environment contribute to various physiological and pathological processes,[23,24] our finding that limb immobilization for a relatively short time (~10 days) altered the gut microbiota and intestinal environment was unexpected. Our observation that the release of immobilization returned the gut microbiota to its original state indicates that the initial effect was primarily induced by

immobilization via an intrinsic mechanism. Whereas extrinsic factors, including the ingestion of food or drugs, influence the gut microbiota, little is known about the intrinsic mechanisms by which the host modulates the gut microbial population. In addition to its effects on immune cell clusters, limb immobilization increased the population size for a progenitor cell cluster, a tuft cell cluster, two of the seven fibroblast-like cell clusters (FB like cells_3 and _6), a mesothelial cell cluster, one of the two enteroendocrine cell clusters (Enteroendocrine cell_1), and an enteric neuron cluster in the intestine. Changes in population size and function of these cell clusters may also have contributed to the immobilization-induced alterations in the intestinal environment and gut microbiota.

Metabolites produced by the gut microbiota play an important role in symbiosis with the host. HYA is a recently discovered LA-derived metabolite produced by gut bacteria and has been detected in human plasma.[12] Whereas the roles of HYA and its related lipid metabolites in the maintenance of human physiological functions are not yet fully understood, evidence suggests that exogenous HYA administration may ameliorate various pathological conditions including chemical colitis, atopic dermatitis, fatty liver disease, and obesity-induced insulin resistance.[25-28] The mechanisms by which HYA exerts such beneficial effects on these conditions, as well as on immobilization-induced muscle inflammation, remain unclear. However, HYA not only attenuates impairment of the intestinal barrier but also interacts with several host proteins including fatty acid receptors.[25] Further elucidation of the detailed mechanisms of HYA action may contribute to the development of its clinical use.

Sympathetic nerves together with immune cells that express adrenergic receptors in the intestine have been implicated in the regulation of tissue damage and repair.[15,16] Adrb1 and Adrb2 expressed in innate lymphoid cells of the small intestine contribute to protection of the tissue against inflammation[29] and to tissue regeneration.[30] The T cell_2 cluster in our analysis appears to correspond to innate lymphoid cells, with the population size for this cell cluster being decreased by limb immobilization. Macrophages that reside in the muscular layer of the intestine exert tissue-protective actions dependent on Adrb2 signaling during bacterial infection.[31,32] We have now shown that *Adrb2* was highly expressed in the Macrophage_1 and _2 clusters, which manifested transcriptional characteristics of anti-inflammatory and pro-inflammatory macrophages, respectively. Macrophage_1 cells therefore likely correspond to macrophages that reside in the muscular layer of the intestine.

Our findings have potential implications for drug development. Given that the safety of HYA administration in humans has been established, we have initiated a

clinical trial of such treatment for individuals prone to the development of muscle atrophy as a result of limb immobilization after orthopedic surgery (clinical trial number: jRCT2051230197). Whereas antibodies to CXCL10 have been shown to be effective for the treatment of inflammatory and cardiovascular conditions in preclinical studies,[33-35] a preventive effect of these antibodies on muscle atrophy has not been reported. Whereas several clinical trials of agents that target CXCL10 have been conducted,[36,37] such agents have yet to be introduced into clinical practice. Given that the upregulation of *CXCL10* expression in muscle was associated with acute limb immobilization not only in the human cohort of the present study but also in a publicly available data set, clinical trials to explore the potential preventive effect of antibodies to CXCL10 on immobilization-induced muscle atrophy are warranted.

In conclusion, our study has revealed a previously unrecognized organ-organ interaction that plays a key role in the development of immobilization-induced muscle atrophy. Two different interventions, both of which are immediately applicable to clinical trials, were shown to be effective for prevention of this condition: the targeting of muscle inflammation with antibodies to CXCL10, and that of intestinal inflammation with HYA. The mechanisms by which limb immobilization signals to the sympathetic nervous system and by which Adrb2 signaling in macrophages induces intestinal inflammation remain to be elucidated. The characterization of these mechanisms may contribute to the further development of new and improved treatments for muscle atrophy.

ACKNOWLEDGMENTS

We thank Akira Suzuki for providing *LysM-Cre* mice, Hidenori Shimizu for gut microbiota analysis, and Yoshika Ogawa for technical assistance. This study was supported in part by grants from Japan Society for the Promotion of Science (KAKENHI grant 22K16397 to Y. Hirata) and Japan Agency for Medical Research and Development (AMED) Practical Research Project for Lifestyle-Related Diseases Including Cardiovascular Diseases and Diabetes Mellitus (23ek0210192h0001 to Y. Hirata, K.N., and W.O.), as well as by grants from Uehara Memorial Foundation, Nakatomi Foundation, Japan Society for the Study of Obesity, and Center for Medical Transformation (all to Y. Hirata) and from Takeda Science Foundation (to W.O.).

AUTHOR CONTRIBUTIONS

Y. Hirata, K.N., and W.O. conceived the study and analyzed the data. K.H., Y. Hosokawa, K.U., T.I., T. Nishigaki, and A.L. contributed to animal and cell experiments.

K.S. contributed to analysis of the public data set. T. Niikura, T.F., K. Oe, and R.K. contributed to analysis of human skeletal muscle. S.H. contributed to gut microbiota and metabolome analysis. S.K. and J.H. contributed to RNA-seq analysis. G.K. contributed to the generation of genetically engineered mice. K. Ohbayashi, T.Y., and Y.I. contributed to measurement of NE turnover. Y. Hirata and W.O. wrote the manuscript.

DECLARATION OF INTERESTS

The authors declare no competing interests.

SUPPLEMENTAL INFORMATION

Document S1. Figures S1–S15 and Tables S1–S3

METHODS

Animals

Adrb2-floxed mice were described previously,[38] and *LysM-Cre* mice[39] were obtained from The Jackson Laboratory (JAX stock #004781). These two mouse lines were crossed to obtain macrophage-specific Adrb2 KO (MΦ-Adrb2KO) mice. All experiments were performed with male mice at 10 weeks of age unless indicated otherwise. Mice were anesthetized by intraperitoneal injection of a mixture of medetomidine (0.3 mg/kg), midazolam (4.0 mg/kg), and butorphanol (5.0 mg/kg) and were then subjected either to bilateral cast-immobilization of hind limbs with the use of plastic tubes, adhesive tape, and animal bandage, or to bilateral hind limb denervation by transection of the sciatic nerve. The immobilized mice were able to move freely around their cages and to obtain food and water using their forelimbs. Animals were analyzed 3 or 10 days after cast-immobilization or denervation unless indicated otherwise. Mice were injected intraperitoneally with neutralizing antibodies to CXCL10 (MAB466, clone 134013; R&D Systems) or control IgG at 0.1 mg/body 3 days before cast-immobilization, or with α-MT (Sigma-Aldrich) at 100 mg/kg, phentolamine (Tokyo Chemical Industry) at 20 mg/kg, or propranolol (Sigma-Aldrich) at 10 mg/kg daily for 10 days concomitant with cast-immobilization. For antibiotic treatment, mice were subjected to oral gavage with a cocktail of ampicillin (5 mg/ml), gentamicin (5 mg/ml), neomycin (5 mg/ml), metronidazole (5 mg/ml), and vancomycin (2.5 mg/ml) daily for 14 days. Diets containing LA, HYD, or HYA (each at 1%) were obtained from Noster and were administered to mice beginning 10 days before immobilization. The separation of blood cells from non–blood cells of skeletal muscle was performed with the use of biotin-conjugated antibodies to mouse CD45.2 (109804, BioLegend), microbeads conjugated with antibodies to biotin (130-090-485, Miltenyi Biotec), and an autoMACS Pro Separator (Miltenyi Biotec). The concentration of LPS or CXCL10 in the plasma was measured using the LAL endotoxin assay kit (GenScript) or the mouse CXCL10 DuoSet ELISA kit (R&D Systems).

Cell culture, RT-qPCR analysis, and immunoblot analysis

C2C12 myoblasts were maintained and induced to differentiate into myotubes as described previously,[40] and they were treated with LPS (L3129, Sigma-Aldrich) at 1 μg/ml for 6 h. Isolation of total RNA from cultured myotubes or from mouse or human tissues as well as RT-qPCR analysis were performed as previously described,[40] and the abundance of target mRNAs was normalized by that of 36B4 mRNA. The sequences of mouse and human PCR primers are provided in Tables S2 and S3, respectively.

Immunoblot analysis was performed with antibodies to claudin-1 (2H10D10, Invitrogen) and to GAPDH (M171-7, MBL). Uncropped immunoblots are shown in Figure S15.

Histology and immunohistochemical staining

Skeletal muscle or colon tissue sections were stained with hematoxylin-eosin or subjected to immunohistochemical staining with antibodies to F4/80. Images were acquired with a BZ-X710 fluorescence microscope (Keyence). The area of muscle fibers, depth of crypts, and F4/80-positive area were quantified for each image with the use of ImageJ software (NIH).

Flow cytometry

Skeletal muscle or the colon was minced and digested with 0.2% collagenase type II (Worthington), the digested tissue was passed through 100-μm and 40-μm cell strainers (Falcon), and erythrocytes were eliminated from the filtrate. The remaining cells were exposed to antibodies to mouse CD16/32 (clone 93, 101302; BioLegend) before staining with antibodies to the following proteins: CD45.2 (clone 104, 109822; BioLegend), Ly6G (clone 1A8, 127606; BioLegend), F4/80 (clone BM8, 123116; BioLegend), CD11b (clone M1/70, 101224; BioLegend), CD11c (clone N418, 117308; BioLegend), and CD206 (clone C068C2, 141720; BioLegend). Dead cells were excluded by staining with propidium iodide (421301, BioLegend). Events were acquired with an LSR Fortessa X-20 instrument (BD Biosciences) and analyzed with FlowJo software (BD Biosciences).

DNA microarray analysis

Total RNA extracted from gastrocnemius muscle of mice at 3 days after cast immobilization or of corresponding control animals was subjected to hybridization with an Affymetrix Mouse Gene 2.0 ST Array.

RNA□seq and scRNA□seq analysis

Total RNA extracted from gastrocnemius muscle or colon tissue was subjected to RNA-seq analysis by Macrogen. A paired-end library was prepared from each RNA sample with the use of a TruSeq Stranded mRNA Library Preparation Kit and was sequenced with a NovaSeq 6000 system (Illumina). Data were analyzed with RaNA-Seq[41] and DAVID Bioinformatics Resources 6.8. A Chromium Next GEM Single Cell Fixed RNA Sample Preparation Kit was used to isolate cells from colon

tissue, and an scRNA-seq library was generated with a 10x Chromium system. Data analysis was performed by Genble.

Gut microbiota and metabolome analysis

DNA was extracted from feces with the use of a QIAamp PowerFecal Pro DNA Kit (Qiagen). For analysis of 16S rRNA genes of the gut microbiota, the V3-V4 region of the gene was amplified from the extracted DNA with 341F (5′-TCGTCGGCAGCGTCAGATGTGTATAAGCGACAGCCTACGGGNGGCWGCAG-3′) and 805R (5′-GTCTCGTGGGCTCGGAGATGTGTATAAGAGACAGGACTACHVGGGTATCTAATCC-3′) primers. Both ends of the amplified fragments were tagged with the use of a Nextera XT Index Kit v2 (Illumina), and the amplicons were then purified and sequenced with the use of an Illumina MiSeq system and MiSeq Reagent Kit v3. Postsequencing analysis was performed with the Quantitative Insights Into Microbial Ecology 2 (QIIME2) pipeline. SILVA (version SSU138.1) was adopted as a reference sequence database for estimation of bacterial species prevalence, and gut microbiota composition was determined with OTUs, which grouped reads with a sequence identity of ≥97%. Comprehensive analysis of gut microbial lipid metabolites was performed as previously described.[42]

Measurement of NE turnover

NE turnover was measured on the basis of the decline in tissue NE content after inhibition of catecholamine biosynthesis with α-MT as described previously.[17,18] Mice were injected intraperitoneally with α-MT at 300 mg/kg. At 0 or 4 h after α-MT injection, the animals were decapitated and tissues were rapidly removed and weighed. Tissue samples were homogenized in 0.2 M perchloric acid containing 0.1 mM EDTA, the homogenate was centrifuged at 4°C, and NE was purified from the resulting supernatant with activated alumina and measured by high-performance liquid chromatography with electrochemical detection. Data are expressed as picograms of NE per milligram of tissue weight.

Human skeletal muscle samples

Specimens of human skeletal muscle were obtained as previously described.[6] In brief, samples were obtained from 15 individuals at an average of 8.3 ± 3.1 days after fixation surgery for a bone fracture of the arm or leg as well as from 18 control participants who underwent implant-removal surgery 6 to 12 months after fixation surgery.

Publicly available human gene expression data analysis

For the analysis of publicly available human gene expression data (Figure S3D), the process of data set selection was undertaken as follows. NCBI GEO and Array Express databases were searched with the terms “muscle”, “cast”, “immobilization”, and “human”. Screening of the three identified data sets resulted in the exclusion of one (GSE45462) because it included only individuals with fractures. The remaining two data sets (GSE14901 and GSE8872) underwent eligibility assessment, with GSE8872 being subsequently excluded on the basis of a small number of healthy subjects ($n = 2$). The remaining data set (GSE14901) met all the inclusion criteria and was adopted for analysis.

Statistical analysis

Quantitative data were presented as means ± SEM or as medians with the interquartile range, and they were analyzed by the two-tailed unpaired Student’s *t* test, two-way analysis of variance (ANOVA) with Bonferroni’s post hoc test, the Mann-Whitney *U* test, or one-way ANOVA followed by Dunnett’s test or Bonferroni’s post hoc test. A p value of <0.05 was considered statistically significant. All statistical analysis was performed with the use of GraphPad Prism 9 (GraphPad Software).

Study approval

All animal experiments were approved by the animal experimentation committee of Kobe University Graduate School of Medicine (approval no. P221201). Human experiments were approved by the medical ethics committee of Kobe University Graduate School of Medicine (approval no. 180059), and all subjects provided written informed consent.

Data availability

The microarray data have been deposited in NCBI Gene Expression Omnibus (GEO) under the accession number GSE172501. The RNA-seq data have been deposited in NCBI GEO under the accession numbers GSE249515 (mouse gastrocnemius) and GSE249324 (mouse colon). The scRNA-seq data have been deposited in NCBI GEO under the accession number GSE265821.

REFERENCES

1. Kalyani, R.R., Corriere, M. & Ferrucci, L. Age-related and disease-related muscle loss: the effect of diabetes, obesity, and other diseases. *Lancet Diabetes Endocrinol* **2**, 819-829 (2014).
2. Cartee, G.D., Hepple, R.T., Bamman, M.M. & Zierath, J.R. Exercise Promotes Healthy Aging of Skeletal Muscle. *Cell Metab.* **23**, 1034-1047 (2016).
3. Preobrazenski, N., Seigel, J., Halliday, S., Janssen, I. & McGlory, C. Single-leg disuse decreases skeletal muscle strength, size, and power in uninjured adults: A systematic review and meta-analysis. *J Cachexia Sarcopenia Muscle* **14**, 684-696 (2023).
4. Gao, Y., Arfat, Y., Wang, H. & Goswami, N. Muscle Atrophy Induced by Mechanical Unloading: Mechanisms and Potential Countermeasures. *Front. Physiol.* **9**, 235 (2018).
5. Hardy, E.J.O., *et al.* The time course of disuse muscle atrophy of the lower limb in health and disease. *J Cachexia Sarcopenia Muscle* **13**, 2616-2629 (2022).
6. Hirata, Y., *et al.* A Piezo1/KLF15/IL-6 axis mediates immobilization-induced muscle atrophy. *J. Clin. Invest.* **132**, 1-13 (2022).
7. Saitou, K., *et al.* Local cyclical compression modulates macrophage function in situ and alleviates immobilization-induced muscle atrophy. *Clin. Sci. (Lond.)* **132**, 2147-2161 (2018).
8. Kawanishi, N., Funakoshi, T. & Machida, S. Time-course study of macrophage infiltration and inflammation in cast immobilization-induced atrophied muscle of mice. *Muscle Nerve* **57**, 1006-1013 (2018).
9. Kawano, Y., *et al.* Colonic Pro-inflammatory Macrophages Cause Insulin Resistance in an Intestinal Ccl2/Ccr2-Dependent Manner. *Cell Metab.* **24**, 295-310 (2016).
10. Tilg, H., Zmora, N., Adolph, T.E. & Elinav, E. The intestinal microbiota fuelling metabolic inflammation. *Nat. Rev. Immunol.* **20**, 40-54 (2020).
11. Garcia-Hernandez, V., Quiros, M. & Nusrat, A. Intestinal epithelial claudins: expression and regulation in homeostasis and inflammation. *Ann. N. Y. Acad. Sci.* **1397**, 66-79 (2017).
12. Kishino, S., *et al.* Polyunsaturated fatty acid saturation by gut lactic acid bacteria affecting host lipid composition. *Proc. Natl. Acad. Sci. U. S. A.* **110**, 17808-17813 (2013).
13. Miyamoto, J., *et al.* A gut microbial metabolite of linoleic acid, 10-hydroxy-cis-12-octadecenoic acid, ameliorates intestinal epithelial barrier impairment partially via GPR40-MEK-ERK pathway. *J. Biol. Chem.* **290**, 2902-2918

608 (2015).
609 14. Hirata, A., *et al.* A novel unsaturated fatty acid hydratase toward C16 to C22 fatty
610 acids from Lactobacillus acidophilus. *J. Lipid Res.* **56**, 1340-1350 (2015).
611 15. Yang, D., Almanzar, N. & Chiu, I.M. The role of cellular and molecular
612 neuroimmune crosstalk in gut immunity. *Cell. Mol. Immunol.* **20**, 1259-1269 (2023).
613 16. Populin, L., Stebbing, M.J. & Furness, J.B. Neuronal regulation of the gut immune
614 system and neuromodulation for treating inflammatory bowel disease. *FASEB*
615 *Bioadv* **3**, 953-966 (2021).
616 17. Saito, M., Minokoshi, Y. & Shimazu, T. Accelerated norepinephrine turnover in
617 peripheral tissues after ventromedial hypothalamic stimulation in rats. *Brain Res.*
618 **481**, 298-303 (1989).
619 18. Shiuchi, T., *et al.* Hypothalamic orexin stimulates feeding-associated glucose
620 utilization in skeletal muscle via sympathetic nervous system. *Cell Metab.* **10**,
621 466-480 (2009).
622 19. Kuramoto, N., *et al.* Role of PDK1 in skeletal muscle hypertrophy induced by
623 mechanical load. *Sci. Rep.* **11**, 3447 (2021).
624 20. Lynch, G.S. & Ryall, J.G. Role of beta-adrenoceptor signaling in skeletal muscle:
625 implications for muscle wasting and disease. *Physiol. Rev.* **88**, 729-767 (2008).
626 21. Wang, X., Yu, L. & Wu, A.R. The effect of methanol fixation on single-cell RNA
627 sequencing data. *BMC Genomics* **22**, 420 (2021).
628 22. van Eijck, C.W.F., *et al.* Enhanced antitumour immunity following neoadjuvant
629 chemoradiotherapy mediates a favourable prognosis in women with resected
630 pancreatic cancer. *Gut* **73**, 311-324 (2024).
631 23. Armet, A.M., *et al.* Rethinking healthy eating in light of the gut microbiome. *Cell*
632 *Host Microbe* **30**, 764-785 (2022).
633 24. Brown, E.M., Clardy, J. & Xavier, R.J. Gut microbiome lipid metabolism and its
634 impact on host physiology. *Cell Host Microbe* **31**, 173-186 (2023).
635 25. Miyamoto, J., *et al.* Gut microbiota confers host resistance to obesity by metabolizing
636 dietary polyunsaturated fatty acids. *Nat Commun* **10**, 4007 (2019).
637 26. Kaikiri, H., *et al.* Supplemental feeding of a gut microbial metabolite of linoleic acid,
638 10-hydroxy-cis-12-octadecenoic acid, alleviates spontaneous atopic dermatitis and
639 modulates intestinal microbiota in NC/nga mice. *Int. J. Food Sci. Nutr.* **68**, 941-951
640 (2017).
641 27. Kasahara, N., *et al.* A gut microbial metabolite of linoleic acid ameliorates liver
642 fibrosis by inhibiting TGF-beta signaling in hepatic stellate cells. *Sci. Rep.* **13**, 18983
643 (2023).

644 28. Yamada, M., *et al.* A bacterial metabolite ameliorates periodontal pathogen-induced
645 gingival epithelial barrier disruption via GPR40 signaling. *Sci. Rep.* **8**, 9008 (2018).
646 29. Moriyama, S., *et al.* beta(2)-adrenergic receptor-mediated negative regulation of
647 group 2 innate lymphoid cell responses. *Science* **359**, 1056-1061 (2018).
648 30. Wang, P., *et al.* Adrenergic nerves regulate intestinal regeneration through IL-22
649 signaling from type 3 innate lymphoid cells. *Cell Stem Cell* **30**, 1166-1178 e1168
650 (2023).
651 31. Gabanyi, I., *et al.* Neuro-immune Interactions Drive Tissue Programming in
652 Intestinal Macrophages. *Cell* **164**, 378-391 (2016).
653 32. Matheis, F., *et al.* Adrenergic Signaling in Muscularis Macrophages Limits
654 Infection-Induced Neuronal Loss. *Cell* **180**, 64-78 e16 (2020).
655 33. Galzi, J.L., *et al.* Neutralizing endogenous chemokines with small molecules.
656 Principles and potential therapeutic applications. *Pharmacol. Ther.* **126**, 39-55
657 (2010).
658 34. van den Borne, P., Quax, P.H., Hoefer, I.E. & Pasterkamp, G. The multifaceted
659 functions of CXCL10 in cardiovascular disease. *Biomed Res Int* **2014**, 893106 (2014).
660 35. Sasaki, Y., *et al.* Blockade of the CXCR3/CXCL10 axis ameliorates inflammation
661 caused by immunoproteasome dysfunction. *JCI Insight* **7**(2022).
662 36. Yellin, M., *et al.* A phase II, randomized, double-blind, placebo-controlled study
663 evaluating the efficacy and safety of MDX-1100, a fully human anti-CXCL10
664 monoclonal antibody, in combination with methotrexate in patients with rheumatoid
665 arthritis. *Arthritis Rheum.* **64**, 1730-1739 (2012).
666 37. Alex Klarenbeek, D.M., Christophe Blanchetot, Michael Saunders, Sebastian van
667 der Woning, Martine Smit, Hans de Haard, Erik Hofman. Targeting chemokines and
668 chemokine receptors with antibodies. *Drug Discov Today Technol* **9**, e227-314 (2012).
669 38. Hinoi, E., *et al.* The sympathetic tone mediates leptin's inhibition of insulin
670 secretion by modulating osteocalcin bioactivity. *J. Cell Biol.* **183**, 1235-1242 (2008).
671 39. Clausen, B.E., Burkhardt, C., Reith, W., Renkawitz, R. & Forster, I. Conditional
672 gene targeting in macrophages and granulocytes using LysMcre mice. *Transgenic*
673 *Res.* **8**, 265-277 (1999).
674 40. Hirata, Y., *et al.* Hyperglycemia induces skeletal muscle atrophy via a WWP1/KLF15
675 axis. *JCI Insight* **4**(2019).
676 41. Prieto, C. & Barrios, D. RaNA-Seq: Interactive RNA-Seq analysis from FASTQ files
677 to functional analysis. *Bioinformatics* (2019).
678 42. Tsuji, K., Shimada, W., Kishino, S., Ogawa, J. & Arita, M. Comprehensive analysis of
679 fatty acid metabolites produced by gut microbiota using LC-MS/MS-based lipidomics.

Medical Mass Spectrometry **6**, 112-125 (2022).

FIGURE LEGENDS

Figure 1. Transition from protein catabolism to inflammation during skeletal muscle immobilization

(A) Ratio of gastrocnemius muscle mass for both hind limbs to body mass for mice subjected to bilateral hind limb immobilization (IM) by cast-fixation for the indicated times (n = 4 mice).

(B–D) Hematoxylin-eosin (HE) staining and immunohistochemical staining of F4/80 (B) for determination of muscle fiber area (C) and the F4/80-positive area (D) in soleus muscle of mice subjected to hind limb immobilization for the indicated times (n = 4 mice). The area of 800 fibers pooled from four mice was measured and averaged for each condition in (C). Scale bar (B), 50 μm.

(E and F) Representative flow cytometric analysis (E) and the percentage (F) of $CD11b^{+}F4/80^{+}$ cells among $CD45^{+}Ly6G^{-}$ cells in immobilized skeletal muscle (n = 4 mice).

(G) RT-qPCR analysis of protein catabolism– or inflammation-related gene expression in gastrocnemius muscle of immobilized mice (n = 4 mice).

(H and I) Kyoto Encyclopedia of Genes and Genomes (KEGG) pathway analysis for RNA-seq data from the gastrocnemius at 3 days (H) or 10 days (I) after hind limb immobilization. The top eight pathways enriched among genes whose expression was upregulated by immobilization are shown.

Quantitative data in (A), (D), (F), and (G) are means ± SEM. *p < 0.05, **p < 0.01, NS (not significant) compared with day 0 (A and G) or as indicated (C, D, and F) by two-way ANOVA with the Bonferroni post hoc test.

See also Figures S1 and S2.

Figure 2. CXCL10 mediates inflammation and atrophy of muscle induced by limb immobilization

(A and B) Volcano plot of RNA-seq data (A) and heat map of inflammation-related gene expression determined by DNA microarray analysis (B) for gastrocnemius of mice subjected to cast-immobilization for 3 days compared with control mice.

(C) RT-qPCR analysis of *Cxcl10* mRNA abundance in gastrocnemius of cast-immobilized mice (n = 4 mice).

(D) Plasma concentration of CXCL10 in cast-immobilized mice (n = 5 mice).

(E) RT-qPCR analysis of *CXCL10* mRNA in skeletal muscle of human individuals subjected to cast-fixation (n = 15) or of control subjects (n = 18).

(F–J) Hematoxylin-eosin and F4/80 immunohistochemical staining (F) and the F4/80-positive area (G) of soleus (n = 4 mice), RT-qPCR analysis of inflammation-related gene expression in gastrocnemius (n = 10 mice) (H), the ratio of muscle mass to body mass (n = 10 mice) (I), and muscle fiber area in soleus (n = 4 mice) (J) for control mice or mice subjected to intraperitoneal injection of neutralizing antibodies to CXCL10 (0.1 mg/body) or control immunoglobulin G (IgG) 3 days before cast-immobilization for 10 days. Scale bar (F), 50 μm. The area of 800 fibers pooled from four mice was measured and averaged for each condition in (J).
Quantitative data are presented as means ± SEM (C, D, G, H, and I) or as box-and-whisker plots (E and J). *$p < 0.05$, **$p < 0.01$, NS relative to day 0 (C and D) or as indicated (E and G–J) by the Mann-Whitney U test (E) or two-way ANOVA with the Bonferroni post hoc test (C, D, and G–J).
See also Figure S3.

Figure 3. Prolonged limb immobilization induces inflammation in the intestine
(A–F) Representative images of the entire intestine (A), length of the small intestine and colon (B), mass of the cecum (C), and hematoxylin-eosin and F4/80 immunohistochemical staining (D) for determination of crypt depth (E) and the F4/80-positive area (F) in the colon of control mice or mice subjected to cast-immobilization for 10 days (n = 4 mice). Scale bars, 2 cm (A) and 50 μm (D). The depth of 100 crypts pooled from four mice was measured and averaged for each condition in (E).
(G and H) Representative flow cytometric analysis (G) and the percentage (H) of $CD11b^{+}F4/80^{+}$ cells among $CD45^{+}Ly6G^{-}$ cells in the colon of immobilized and control mice (n = 4 mice).
(I) GSEA of RNA-seq data obtained from the colon of immobilized and control mice.
(J and K) Immunoblot analysis of claudin-1 and GAPDH (loading control) in the colon (n = 6 mice) (J) and the plasma concentration of LPS (n = 4 mice) (K) for mice subjected (or not) to cast-immobilization for 10 days.
(L) RT-qPCR analysis of *Cxcl10* mRNA abundance in C2C12 myotubes exposed to LPS (1 μg/ml) or vehicle (control) for 6 h (n = 4 independent experiments).
Quantitative data are presented as means ± SEM (B, C, F, H, and J–L) or as box-and-whisker plots (E). *$p < 0.05$, **$p < 0.01$ (unpaired Student's t test).
See also Figures S4 , S5, and S15.

Figure 4. The gut microbiota contributes to inflammation and atrophy of skeletal

muscle induced by immobilization

(A–C) Gut microbial composition at the genus level determined by analysis of bacterial 16S rRNA genes (A), relative abundance of the Lachnospiraceae group and *Lactobacillus* species (B), and corresponding principal component (PC) analysis (C) for control mice or mice subjected to cast-immobilization for 10 days (n = 6 mice).

(D and E) Ratio of soleus muscle mass to body mass (D) and RT-qPCR analysis of inflammation-related gene expression in gastrocnemius (E) for control or cast-immobilized mice treated with a cocktail of antibiotics (Abx) or vehicle by oral gavage daily for 14 days (n = 6 mice).

Quantitative data are presented as the mean ± SEM (D and E) or the median and interquartile range (B). *$p < 0.05$, **$p < 0.01$, NS by the Mann-Whitney U test (B) or two-way ANOVA with the Bonferroni post hoc test (D and E).

See also Figure S6.

Figure 5. A gut microbial metabolite derived from LA inhibits intestinal and muscle inflammation as well as muscle atrophy induced by limb immobilization

(A–C) Hematoxylin-eosin and F4/80 immunohistochemical staining (A) for determination of crypt depth (B) and the F4/80-positive area (C) in the colon of mice fed a normal diet (ND) or a diet containing LA, HYD, or HYA and subjected (or not) to cast-fixation of the hind limbs for 10 days (n = 6 mice). The depth of 100 crypts pooled from four mice was measured and averaged for each condition in (B). Scale bar (A), 50 µm.

(D and E) Ratio of muscle mass to body mass (D) as well as hematoxylin-eosin and F4/80 immunohistochemical staining (E) for the soleus of mice (n = 6) treated as in (A) to (C). Scale bar (E), 50 µm.

Quantitative data are means ± SEM (C and D) or are presented as box-and-whisker plots (B). *$p < 0.05$, **$p < 0.01$ (two-way ANOVA with the Bonferroni post hoc test).

See also Figures S7 to S11.

Figure 6. Sympathetic nerve activation contributes to intestinal inflammation induced by limb immobilization

(A and B) NE content (A) and relative NE content (at 4 h versus 0 h) (B) for the stomach, duodenum, proximal and distal small intestine, and colon of control or cast-immobilized (10 days) mice at 0 and 4 h after intraperitoneal (ip) injection of α-MT (n = 6 mice).

(C) Heat map for the expression of adrenergic receptor genes in the colon of mice fed a

normal diet or a diet containing HYA and subjected (or not) to cast-immobilization for 10 days (n = 3 mice).

(D) RT-qPCR analysis of inflammation-related gene expression in the distal small intestine of mice subjected to intraperitoneal injection of α-MT, phentolamine, propranolol, or vehicle daily for 10 days with or without concomitant cast-immobilization (n = 6 mice).

(E) Uniform manifold approximation and projection (UMAP) representation of 37 cell clusters identified by scRNA-seq analysis of the colon for control mice or mice subjected to cast-immobilization for 10 days. DC, dendritic cell; EEC, enteroendocrine cell; FB, fibroblast.

(F) Percentage of the indicated cell clusters among all cells. Red or blue squares indicate cell clusters for which cast-immobilization increased or decreased the cell ratio by >20%, respectively.

(G) Feature plot of *Adrb2* expression in the cell clusters of the colon.

Quantitative data in (A), (B), and (D) are means ± SEM. *p < 0.05, **p < 0.01, NS by the unpaired Student's t test (B) or two-way ANOVA with the Bonferroni post hoc test (A and D).

See also Figures S12 and S13 as well as Table S1.

Figure 7. Prevention of β2-adrenergic signaling in macrophages attenuates intestinal and muscle inflammation induced by prolonged limb immobilization

(A–H) Percentage of the indicated cell clusters among all cells in the colon as determined by scRNA-seq analysis (A); representative flow cytometric analysis (B) and the percentage (n = 4 mice) (C) of $CD11b^{+}F4/80^{+}$ cells among $CD45^{+}Ly6G^{-}$ cells in the colon; F4/80 immunohistochemical staining of the colon (D) for determination of crypt depth (n = 4 mice) (E) and the F4/80-positive area (n = 4 mice) (F); the percentage of $CD11b^{+}F4/80^{+}$ cells among $CD45^{+}Ly6G^{-}$ cells in hind limb skeletal muscle (n = 4 mice) (G); and the ratio of soleus muscle mass to body mass (n = 6 mice) (H) for wild-type (WT) or macrophage-specific Adrb2 KO (MΦ-Adrb2KO) mice subjected (or not) to cast-immobilization for 10 days. The depth of 100 crypts pooled from four mice was measured and averaged for each condition in (E). Scale bar (D), 50 μm. Quantitative data are means ± SEM (C and F–H) or are presented as box-and-whisker plots (E). **p < 0.01, NS (two-way ANOVA with the Bonferroni post hoc test).

(I) Proposed role of a skeletal muscle–sympathetic nerve–intestine network in immobilization-induced muscle inflammation and atrophy.

See also Figures S14 and Table S1.

826

SUPPLEMENTAL FIGURE LEGENDS

Figure S1, related to Figure 1. Gating strategy and immobilization-induced changes in macrophage subsets of skeletal muscle as well as GSEA for immobilized muscle

(A) Gating strategy for fluorescence-activated sorting of macrophages from skeletal muscle of immobilized mice. SSC, side scatter; FSC, forward scatter; PI, propidium iodide.

(B and C) Representative flow cytometric analysis (B) and the percentage (C) of $CD11c^{+}CD206^{-}$ or $CD11c^{-}CD206^{+}$ cells in skeletal muscle of mice subjected to hind limb immobilization by cast-fixation for the indicated times (n = 4 mice). Data in (C) are means ± SEM. $^{**}p < 0.01$, NS (two-way ANOVA with the Bonferroni post hoc test).

(D and E) GSEA for the indicated pathways performed with RNA-seq data from gastrocnemius muscle of mice immobilized for 3 days (D) or 10 days (E). ES, enrichment score.

Figure S2, related to Figure 1. Time course of denervation-induced muscle atrophy, macrophage accumulation, and changes in gene expression

(A) Ratio of gastrocnemius muscle mass in both hind limbs to body mass for mice subjected to bilateral hind limb denervation (Den) for the indicated times (n = 4 mice).

(B–D) Hematoxylin-eosin and F4/80 immunohistochemical staining (B) for determination of muscle fiber area (C) and the F4/80-positive area (D) in soleus muscle of denervated mice (n = 4 mice). The area of 800 fibers pooled from four mice was measured and averaged for each condition in (C). Scale bar (B), 50 μm.

(E) RT-qPCR analysis of protein catabolism– or inflammation-related gene expression in the gastrocnemius of denervated mice (n = 4 mice).

Quantitative data are presented as means ± SEM (A, D, and E) or as box-and-whisker plots (C). $^{*}p < 0.05$, $^{**}p < 0.01$, NS (two-way ANOVA with the Bonferroni post hoc test) versus day 0 (A and E) or as indicated (C and D).

Figure S3, related to Figure 2. Identification of the chemokine CXCL10 as a mediator of muscle inflammation induced by limb immobilization

(A) RT-qPCR analysis of *Cxcl10*, *Ptprc*, and *Myh4* mRNA abundance in the blood cell and non–blood cell fractions of skeletal muscle from cast-immobilized mice (n = 4 mice).

(B) RT-qPCR analysis of *Cxcl10* mRNA in gastrocnemius of denervated mice (n = 4 mice).

(C) RT-qPCR analysis of inflammation-related gene expression in skeletal muscle of control (n = 18) or immobilized (n = 15) human participants.
(D) Relative expression of *CXCL10* in skeletal muscle of healthy human individuals subjected to cast-immobilization as determined from a publicly available data set. The relative expression level is presented as transcripts per million (TPM) for the subjects before (Pre-cast) and at two time points after (Cast_2 days and Cast_14 days) cast application. Each point represents one individual.
(E and F) Ratio of muscle mass to body mass (E) and RT-qPCR analysis of catabolism-related gene expression in gastrocnemius (F) for control mice or mice subjected to intraperitoneal injection of neutralizing antibodies to CXCL10 (0.1 mg/body) or of control IgG at 3 days before cast-immobilization for 3 days (n = 5 mice).
All data are means ± SEM. *p < 0.05, **p < 0.01, NS compared with day 0 (B) or as indicated (A and C–F) by the unpaired Student's t test (A and C), two-way ANOVA with the Bonferroni post hoc test (A, B, E, and F), or one-way ANOVA followed by Dunnett's test (D).

Figure S4, related to Figure 3. Effects of prolonged limb immobilization on intestinal tissue, and gating strategy for macrophage subsets in the colon
(A) Mass of the stomach, duodenum, proximal and distal small intestine, and colon for control mice or mice subjected to cast-immobilization for 10 days (n = 6 mice).
(B and C) Length of the small intestine and colon (B) as well as mass of the cecum (C) for mice subjected to cast-immobilization for the indicated times (n = 4 mice).
(D) Gating strategy for fluorescence-activated sorting of macrophages from the colon of immobilized mice.
(E and F) Representative flow cytometric analysis (E) and the percentage (F) of $CD11c^{+}CD206^{-}$ cells and $CD11c^{-}CD206^{+}$ cells in the colon of cast-immobilized (10 days) and control mice (n = 4 mice).
Quantitative data are means ± SEM. *p < 0.05, **p < 0.01, NS compared with day 0 (B and C) or as indicated (A and F) by the unpaired Student's t test (A and F) or two-way ANOVA with the Bonferroni post hoc test (B and C).

Figure S5, related to Figure 3. Effects of prolonged limb immobilization by cast-fixation or denervation on intestinal tissue
(A) RT-qPCR analysis of inflammation-related gene expression in the proximal or distal small intestine and colon of cast-immobilized (10 days) and control mice (n = 4 mice).

(B and C) Length of the small intestine and colon (B) as well as mass of the cecum (C) for mice subjected to limb denervation for the indicated times (n = 4 mice).
(D) RT-qPCR analysis of inflammation-related gene expression in the proximal or distal small intestine and colon of denervated and control mice (n = 4 mice).
All data are means ± SEM. *p < 0.05, **p < 0.01, NS compared with day 0 (B and C) or as indicated (A and D) by the unpaired Student's t test (A and D) or two-way ANOVA with the Bonferroni post hoc test (B and C).

Figure S6, related to Figure 4. Effects of prolonged limb immobilization by cast-fixation or denervation on the gut microbiota
(A–C) Gut microbial composition at the genus level (A), relative abundance of the Lachnospiraceae group and *Lactobacillus* species (B), and corresponding principal component analysis (C) for control mice and mice subjected to cast immobilization for 10 days with (remobilization) or without subsequent cast removal for 14 days (n = 6 mice).
(D and E) Gut microbial composition at the genus level (D) and relative abundance of the Lachnospiraceae group and *Lactobacillus* species (E) for control mice or mice subjected to hind limb denervation for 10 days (n = 6 mice).
Quantitative data in (B) and (E) are presented as the median and interquartile range. *p < 0.05, **p < 0.01, NS by one-way ANOVA with the Bonferroni post hoc test (B) or the Mann-Whitney U test (E).

Figure S7, related to Figure 5. Prolonged limb immobilization by cast-fixation influences the fecal levels of fatty acid metabolites produced by the gut microbiota
(A) Metabolic pathway of LA showing the structure of fatty acid metabolites.
(B) Fatty acid concentrations in cecal content of mice subjected (or not) to cast-immobilization for 10 days (n = 6 mice). HYC was below the detection limit in most samples. Data are medians with the interquartile range. **p < 0.01, NS (Mann-Whitney U test).

Figure S8, related to Figure 5. Prolonged limb immobilization by denervation influences the fecal levels of fatty acid metabolites produced by the gut microbiota
(A) Fatty acid concentrations in feces of control and denervated mice (10 days) (n = 6 mice). HYC was below the detection limit in all samples.
(B) Daily food intake of mice maintained on a normal diet (ND) or a diet containing LA, HYD, or HYA and subjected (or not) to cast-immobilization for 10 days (n = 6 mice).

Data are medians with the interquartile range (A) or means ± SEM (B). *$p < 0.05$, **$p < 0.01$, NS by the Mann-Whitney *U* test (A) or two-way ANOVA with the Bonferroni post hoc test (B).

Figure S9, related to Figure 5. Effects of HYA on intestinal inflammation induced by prolonged limb immobilization

(A–C) Length of the colon ($n = 6$ mice) (A), RT-qPCR analysis of inflammation-related gene expression in the colon ($n = 6$ mice) (B), and immunoblot analysis of claudin-1 in the colon ($n = 4$ mice) (C) of mice fed a normal diet or a diet containing LA, HYD, or HYA and subjected (or not) to cast-immobilization for 10 days.

All quantitative data are means ± SEM. *$p < 0.05$, **$p < 0.01$, NS (two-way ANOVA with the Bonferroni post hoc test).

See also Figure S15.

Figure S10, related to Figure 5. Effects of HYA on intestinal inflammation induced by prolonged limb immobilization

(A and B) GO functional analysis of RNA-seq data from the colon for biological processes upregulated in mice fed a normal diet and subjected to cast-immobilization for 10 days versus those not subjected to immobilization (A) as well as for biological processes downregulated in immobilized mice fed a diet containing HYA versus those fed a normal diet (B). The top 20 processes enriched among genes whose expression was altered by each condition are shown. p_{adj}, adjusted *p* value.

(C) Plasma concentration of LPS in mice fed a normal diet or a diet containing LA, HYD, or HYA and subjected (or not) to cast-immobilization for 10 days ($n = 4$ mice). Data are means ± SEM. *$p < 0.05$, **$p < 0.01$, NS (two-way ANOVA with the Bonferroni post hoc test).

Figure S11, related to Figure 5. Effects of HYA on muscle inflammation and atrophy induced by prolonged limb immobilization

(A–C) Muscle fiber area (A) and the F4/80-positive area (B) in soleus (determined from images as in Figure 5E) as well as RT-qPCR analysis of inflammation-related gene expression in gastrocnemius (C) for mice fed a normal diet or a diet supplemented with LA, HYD, or HYA and subjected (or not) to cast-immobilization for 10 days ($n = 6$ mice). The area of 400 fibers pooled from four mice was measured and averaged for each condition in (A).

Data are presented as box-and-whisker plots (A) or are means ± SEM (B and C). *$p <$

0.05, **$p < 0.01$, NS (two-way ANOVA with the Bonferroni post hoc test).

Figure S12, related to Figure 6. Sympathetic nerve activation contributes to muscle inflammation induced by limb immobilization

(A and B) RT-qPCR analysis of inflammation-related gene expression in gastrocnemius (n = 6 mice) (A) as well as the ratio of gastrocnemius muscle mass to body mass (n = 4 mice) (B) for mice subjected to intraperitoneal injection of α-MT, phentolamine, propranolol, or vehicle daily for 10 days with or without concomitant cast-immobilization. Data are means ± SEM. *$p < 0.05$, **$p < 0.01$, NS (two-way ANOVA with the Bonferroni post hoc test).

(C) Heat map for the expression of all genes in the cell clusters of the colon identified by scRNA-seq analysis.

Figure S13, related to Figure 6. Heat map for expression of adrenergic receptor genes in cell clusters of the colon as determined by scRNA-seq analysis

Figure S14, related to Figure 7. Intestinal and muscle inflammation induced by prolonged limb immobilization is attenuated in MΦ-Adrb2KO mice

(A–C) Representative flow cytometric analysis (A) and the percentage (B) of $CD11c^{+}CD206^{-}$ cells or $CD11c^{-}CD206^{+}$ cells among $CD11b^{+}F4/80^{+}$ cells as well as RT-qPCR analysis of inflammation-related gene expression (C) in the colon of WT or MΦ-Adrb2KO mice subjected (or not) to cast-immobilization for 10 days (n = 4 mice).

(D–F) Representative flow cytometric analysis of $CD11b^{+}F4/80^{+}$ cells among $CD45^{+}Ly6G^{-}$ cells (D) as well as representative flow cytometric analysis (E) and the percentage (F) of $CD11c^{+}CD206^{-}$ cells or $CD11c^{-}CD206^{+}$ cells among $CD11b^{+}F4/80^{+}$ cells in hind limb skeletal muscle of WT or MΦ-Adrb2KO mice subjected (or not) to cast immobilization for 10 days (n = 4 mice).

All quantitative data are means ± SEM. *$p < 0.05$, **$p < 0.01$, NS (two-way ANOVA with the Bonferroni post hoc test).

Figure S15, related to Figures 3 and S9. Uncropped immunoblot images

Black boxes contain the areas shown in the indicated figures.

Table S1, related to Figures 6 and 7. Genes that characterize cell clusters of the colon identified by scRNA-seq analysis of control mice and mice subjected to cast-immobilization for 10 days

The exocrine cell cluster is characterized by expression of genes for digestive enzymes including *Ctrb1*, *Cela2a*, *Cela3b*, and *Cap1*, all of which are commonly expressed in pancreatic exocrine cells. Moreover, this cluster was detected in a specific sample. Given that this cluster may have been derived from ectopic pancreatic tissue congenitally admixed with intestinal tissue, or from contaminating pancreatic tissue artefactually introduced during intestinal tissue collection, it was excluded from further analysis.

Table S2, related to STAR METHODS. Sequences of mouse primers for RT-qPCR analysis

FWD, forward; REV, reverse.

Table S3, related to STAR METHODS. Sequences of human primers for RT-qPCR analysis

FWD, forward; REV, reverse.

Figure 1

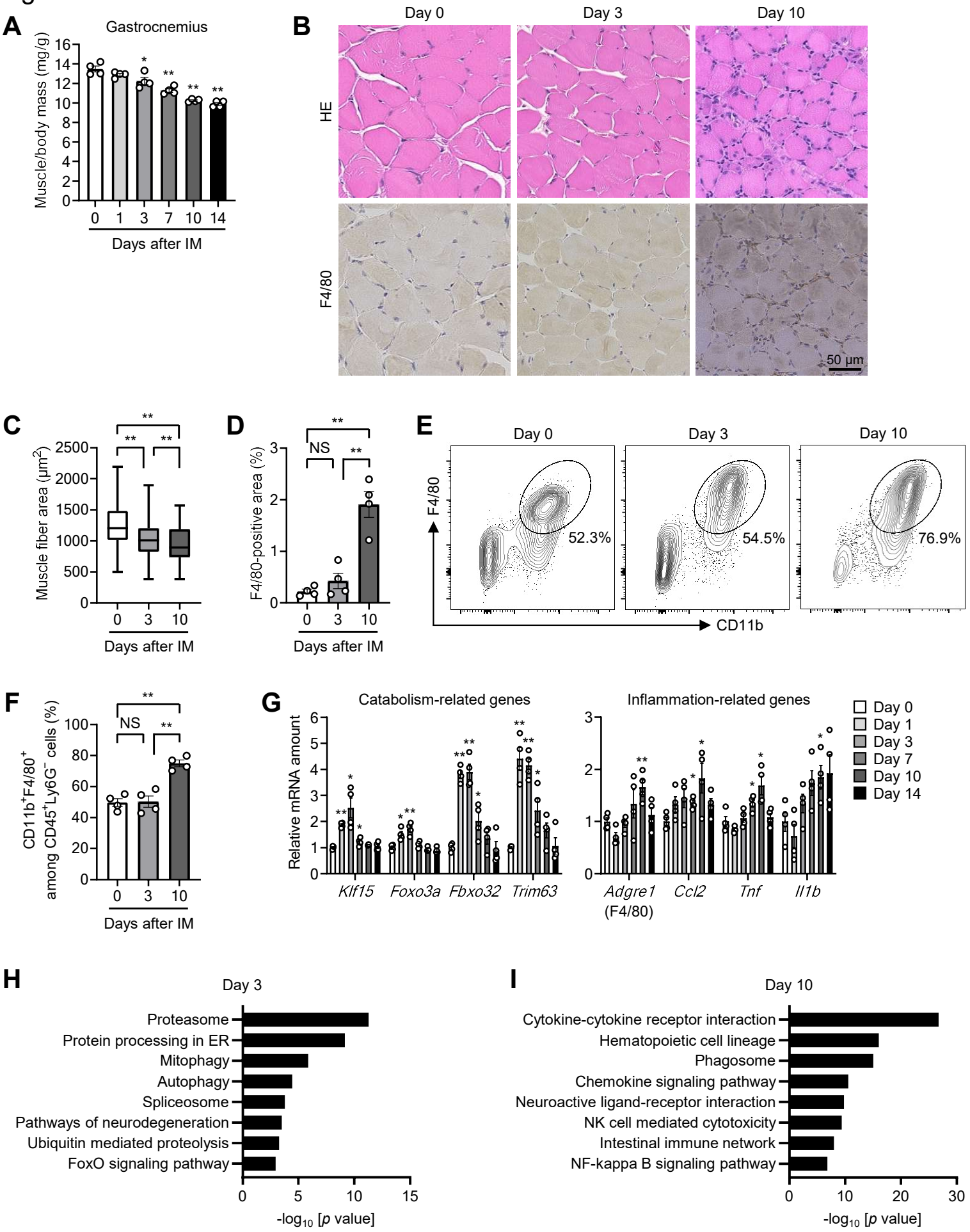
A
Gastrocnemius
Muscle/body mass (mg/g)
Days after IM
B
Day 0
Day 3
Day 10
HE
F4/80
50 μm
C
Muscle fiber area (μm²)
Days after IM
D
F4/80-positive area (%)
NS
Days after IM
E
Day 0
Day 3
Day 10
F4/80
CD11b
52.3%
54.5%
76.9%
F
CD11b⁺F4/80⁺ among CD45⁺Ly6G⁻ cells (%)
NS
Days after IM
G
Catabolism-related genes
Inflammation-related genes
Relative mRNA amount
Klf15
Foxo3a
Fbxo32
Trim63
Adgre1 (F4/80)
Ccl2
Tnf
Il1b
Day 0
Day 1
Day 3
Day 7
Day 10
Day 14
H
Day 3
Proteasome
Protein processing in ER
Mitophagy
Autophagy
Spliceosome
Pathways of neurodegeneration
Ubiquitin mediated proteolysis
FoxO signaling pathway
-log10 [p value]
I
Day 10
Cytokine-cytokine receptor interaction
Hematopoietic cell lineage
Phagosome
Chemokine signaling pathway
Neuroactive ligand-receptor interaction
NK cell mediated cytotoxicity
Intestinal immune network
NF-kappa B signaling pathway
-log10 [p value]

Figure 1. Transition from protein catabolism to inflammation during skeletal muscle immobilization

(A) Ratio of gastrocnemius muscle mass for both hind limbs to body mass for mice subjected to bilateral hind limb immobilization (IM) by cast-fixation for the indicated times (n = 4 mice).

(B–D) Hematoxylin-eosin (HE) staining and immunohistochemical staining of F4/80 (B) for determination of muscle fiber area (C) and the F4/80-positive area (D) in soleus muscle of mice subjected to hind limb immobilization for the indicated times (n = 4 mice). The area of 800 fibers pooled from four mice was measured and averaged for each condition in (C). Scale bar (B), 50 μm.

(E and F) Representative flow cytometric analysis (E) and the percentage (F) of $CD11b^{+}F4/80^{+}$ cells among $CD45^{+}Ly6G^{-}$ cells in immobilized skeletal muscle (n = 4 mice).

(G) RT-qPCR analysis of protein catabolism– or inflammation-related gene expression in gastrocnemius muscle of immobilized mice (n = 4 mice).

(H and I) Kyoto Encyclopedia of Genes and Genomes (KEGG) pathway analysis for RNA-seq data from the gastrocnemius at 3 days (H) or 10 days (I) after hind limb immobilization. The top eight pathways enriched among genes whose expression was upregulated by immobilization are shown.

Quantitative data in (A), (D), (F), and (G) are means ± SEM. *$p < 0.05$, **$p < 0.01$, NS (not significant) compared with day 0 (A and G) or as indicated (C, D, and F) by two-way ANOVA with the Bonferroni post hoc test.

See also Figures S1 and S2.

Figure 2

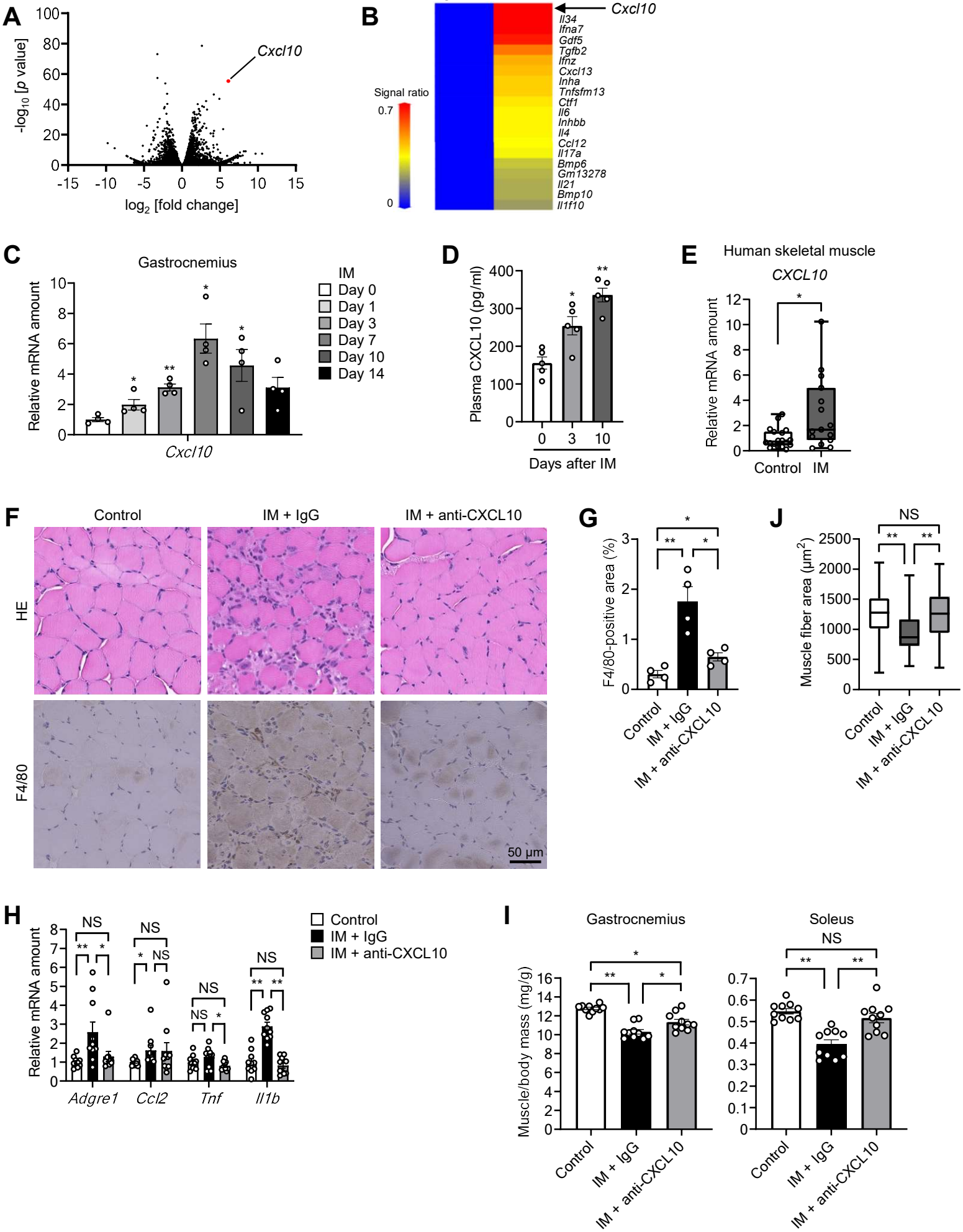
A
-log10 [p value]
log2 [fold change]
Cxcl10
B
Control
IM
Cxcl10
Il34
Ifna7
Gdf5
Tgfb2
Ifnz
Cxcl13
Inha
Tnfsfm13
Ctf1
Il6
Inhbb
Il4
Ccl12
Il17a
Bmp6
Gm13278
Il21
Bmp10
Il1f10
Signal ratio
0.7
0
C
Gastrocnemius
Relative mRNA amount
Cxcl10
IM
Day 0
Day 1
Day 3
Day 7
Day 10
Day 14
D
Plasma CXCL10 (pg/ml)
Days after IM
E
Human skeletal muscle
CXCL10
Relative mRNA amount
Control
IM
F
Control
IM + IgG
IM + anti-CXCL10
HE
F4/80
50 μm
G
F4/80-positive area (%)
Control
IM + IgG
IM + anti-CXCL10
J
Muscle fiber area (μm2)
NS
H
Relative mRNA amount
Adgre1
Ccl2
Tnf
Il1b
Control
IM + IgG
IM + anti-CXCL10
I
Gastrocnemius
Soleus
Muscle/body mass (mg/g)
Control
IM + IgG
IM + anti-CXCL10

Figure 2. CXCL10 mediates inflammation and atrophy of muscle induced by limb immobilization

(A and B) Volcano plot of RNA-seq data (A) and heat map of inflammation-related gene expression determined by DNA microarray analysis (B) for gastrocnemius of mice subjected to cast-immobilization for 3 days compared with control mice.

(C) RT-qPCR analysis of *Cxcl10* mRNA abundance in gastrocnemius of cast-immobilized mice (n = 4 mice).

(D) Plasma concentration of CXCL10 in cast-immobilized mice (n = 5 mice).

(E) RT-qPCR analysis of *CXCL10* mRNA in skeletal muscle of human individuals subjected to cast-fixation (n = 15) or of control subjects (n = 18).

(F–J) Hematoxylin-eosin and F4/80 immunohistochemical staining (F) and the F4/80-positive area (G) of soleus (n = 4 mice), RT-qPCR analysis of inflammation-related gene expression in gastrocnemius (n = 10 mice) (H), the ratio of muscle mass to body mass (n = 10 mice) (I), and muscle fiber area in soleus (n = 4 mice) (J) for control mice or mice subjected to intraperitoneal injection of neutralizing antibodies to CXCL10 (0.1 mg/body) or control immunoglobulin G (IgG) 3 days before cast-immobilization for 10 days. Scale bar (F), 50 μm. The area of 800 fibers pooled from four mice was measured and averaged for each condition in (J).

Quantitative data are presented as means ± SEM (C, D, G, H, and I) or as box-and-whisker plots (E and J). *$p < 0.05$, **$p < 0.01$, NS relative to day 0 (C and D) or as indicated (E and G–J) by the Mann-Whitney U test (E) or two-way ANOVA with the Bonferroni post hoc test (C, D, and G–J).

See also Figure S3.

Figure 3

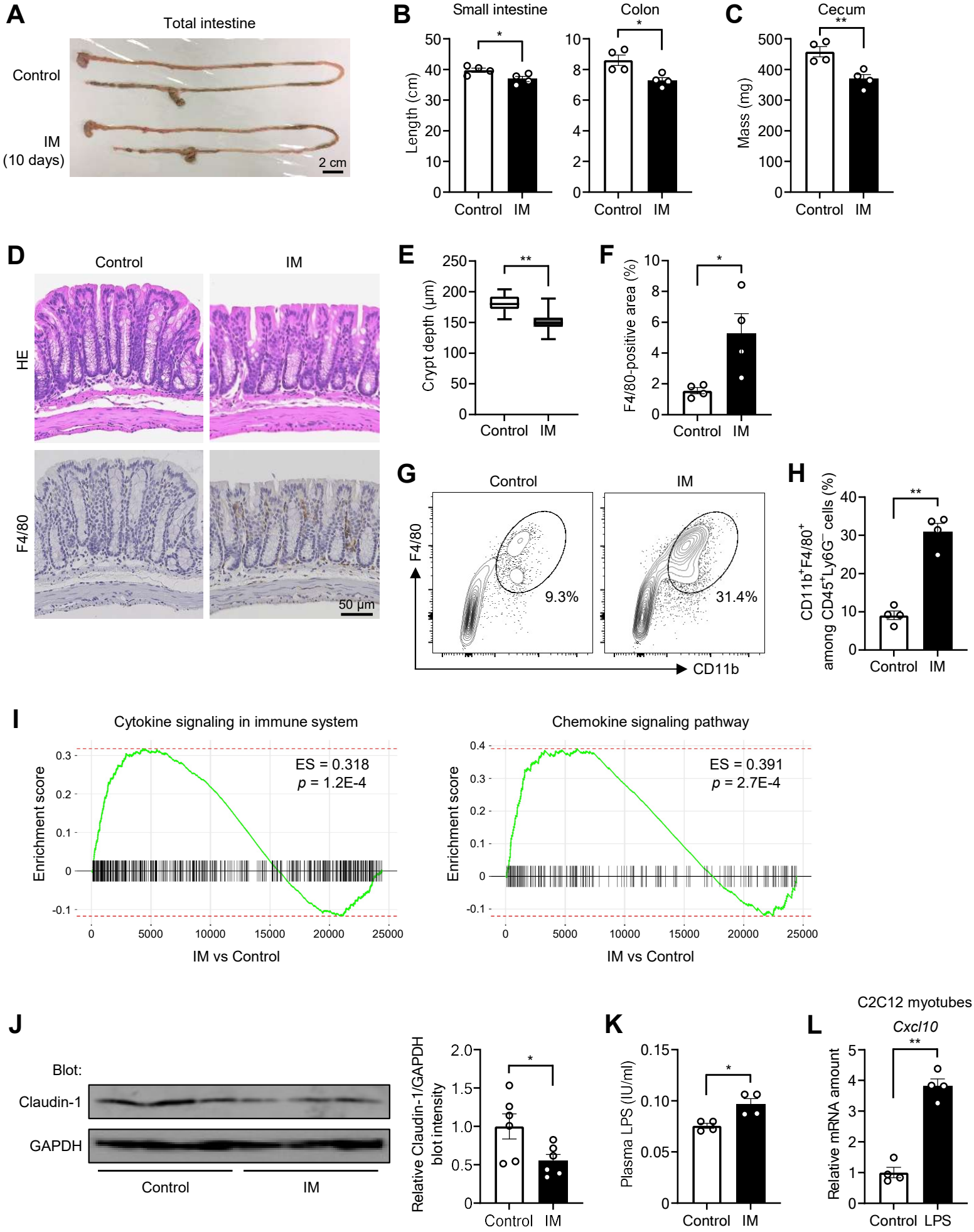
A
Total intestine
Control
IM
(10 days)
2 cm
B
Small intestine
Colon
Length (cm)
Control
IM
C
Cecum
Mass (mg)
D
Control
IM
HE
F4/80
50 μm
E
Crypt depth (μm)
F
F4/80-positive area (%)
G
F4/80
CD11b
9.3%
31.4%
H
CD11b+F4/80+ among CD45+Ly6G− cells (%)
I
Cytokine signaling in immune system
ES = 0.318
p = 1.2E-4
Enrichment score
IM vs Control
Chemokine signaling pathway
ES = 0.391
p = 2.7E-4
J
Blot:
Claudin-1
GAPDH
Relative Claudin-1/GAPDH blot intensity
K
Plasma LPS (IU/ml)
L
C2C12 myotubes
Cxcl10
Relative mRNA amount
LPS

Figure 3. Prolonged limb immobilization induces inflammation in the intestine
(A–F) Representative images of the entire intestine (A), length of the small intestine and colon (B), mass of the cecum (C), and hematoxylin-eosin and F4/80 immunohistochemical staining (D) for determination of crypt depth (E) and the F4/80-positive area (F) in the colon of control mice or mice subjected to cast-immobilization for 10 days (n = 4 mice). Scale bars, 2 cm (A) and 50 μm (D). The depth of 100 crypts pooled from four mice was measured and averaged for each condition in (E).
(G and H) Representative flow cytometric analysis (G) and the percentage (H) of $CD11b^{+}F4/80^{+}$ cells among $CD45^{+}Ly6G^{-}$ cells in the colon of immobilized and control mice (n = 4 mice).
(I) GSEA of RNA-seq data obtained from the colon of immobilized and control mice.
(J and K) Immunoblot analysis of claudin-1 and GAPDH (loading control) in the colon (n = 6 mice) (J) and the plasma concentration of LPS (n = 4 mice) (K) for mice subjected (or not) to cast-immobilization for 10 days.
(L) RT-qPCR analysis of *Cxcl10* mRNA abundance in C2C12 myotubes exposed to LPS (1 μg/ml) or vehicle (control) for 6 h (n = 4 independent experiments).
Quantitative data are presented as means ± SEM (B, C, F, H, and J–L) or as box-and-whisker plots (E). *$p < 0.05$, **$p < 0.01$ (unpaired Student's t test).
See also Figures S4 , S5, and S15.

Figure 4

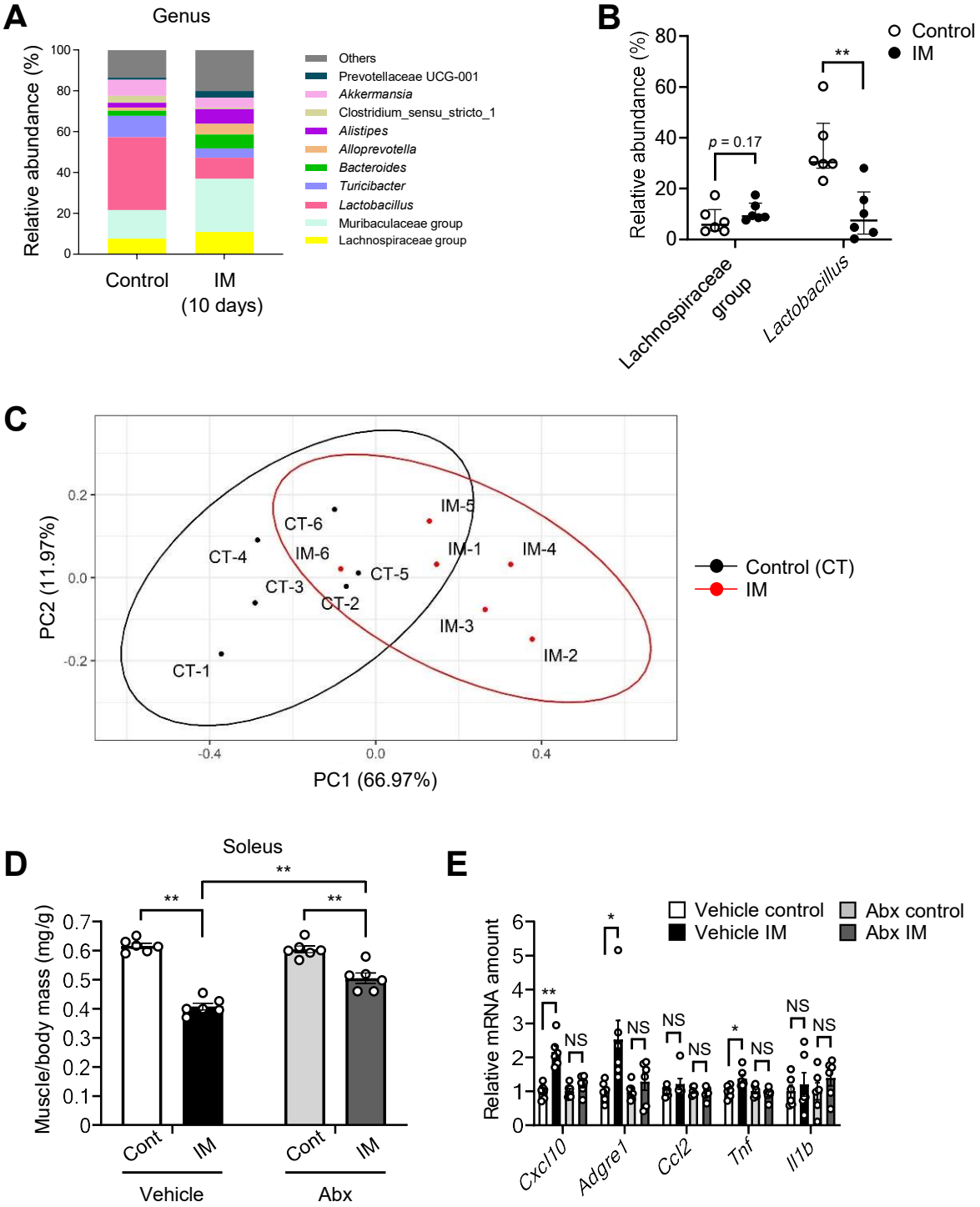
A
Genus
Relative abundance (%)
Control
IM
(10 days)
Others
Prevotellaceae UCG-001
Akkermansia
Clostridium_sensu_stricto_1
Alistipes
Alloprevotella
Bacteroides
Turicibacter
Lactobacillus
Muribaculaceae group
Lachnospiraceae group
B
Control
IM
Relative abundance (%)
p = 0.17
**
Lachnospiraceae group
Lactobacillus
C
PC2 (11.97%)
PC1 (66.97%)
CT-1
CT-2
CT-3
CT-4
CT-5
CT-6
IM-1
IM-2
IM-3
IM-4
IM-5
IM-6
Control (CT)
IM
D
Soleus
Muscle/body mass (mg/g)
Cont
IM
Vehicle
Abx
E
Vehicle control
Vehicle IM
Abx control
Abx IM
Relative mRNA amount
Cxcl10
Adgre1
Ccl2
Tnf
Il1b
NS

Figure 4. The gut microbiota contributes to inflammation and atrophy of skeletal muscle induced by immobilization

(A–C) Gut microbial composition at the genus level determined by analysis of bacterial 16S rRNA genes (A), relative abundance of the Lachnospiraceae group and *Lactobacillus* species (B), and corresponding principal component (PC) analysis (C) for control mice or mice subjected to cast-immobilization for 10 days (n = 6 mice).

(D and E) Ratio of soleus muscle mass to body mass (D) and RT-qPCR analysis of inflammation-related gene expression in gastrocnemius (E) for control or cast-immobilized mice treated with a cocktail of antibiotics (Abx) or vehicle by oral gavage daily for 14 days (n = 6 mice).

Quantitative data are presented as the mean ± SEM (D and E) or the median and interquartile range (B). *$p < 0.05$, **$p < 0.01$, NS by the Mann-Whitney U test (B) or two-way ANOVA with the Bonferroni post hoc test (D and E).

See also Figure S6.

Figure 5

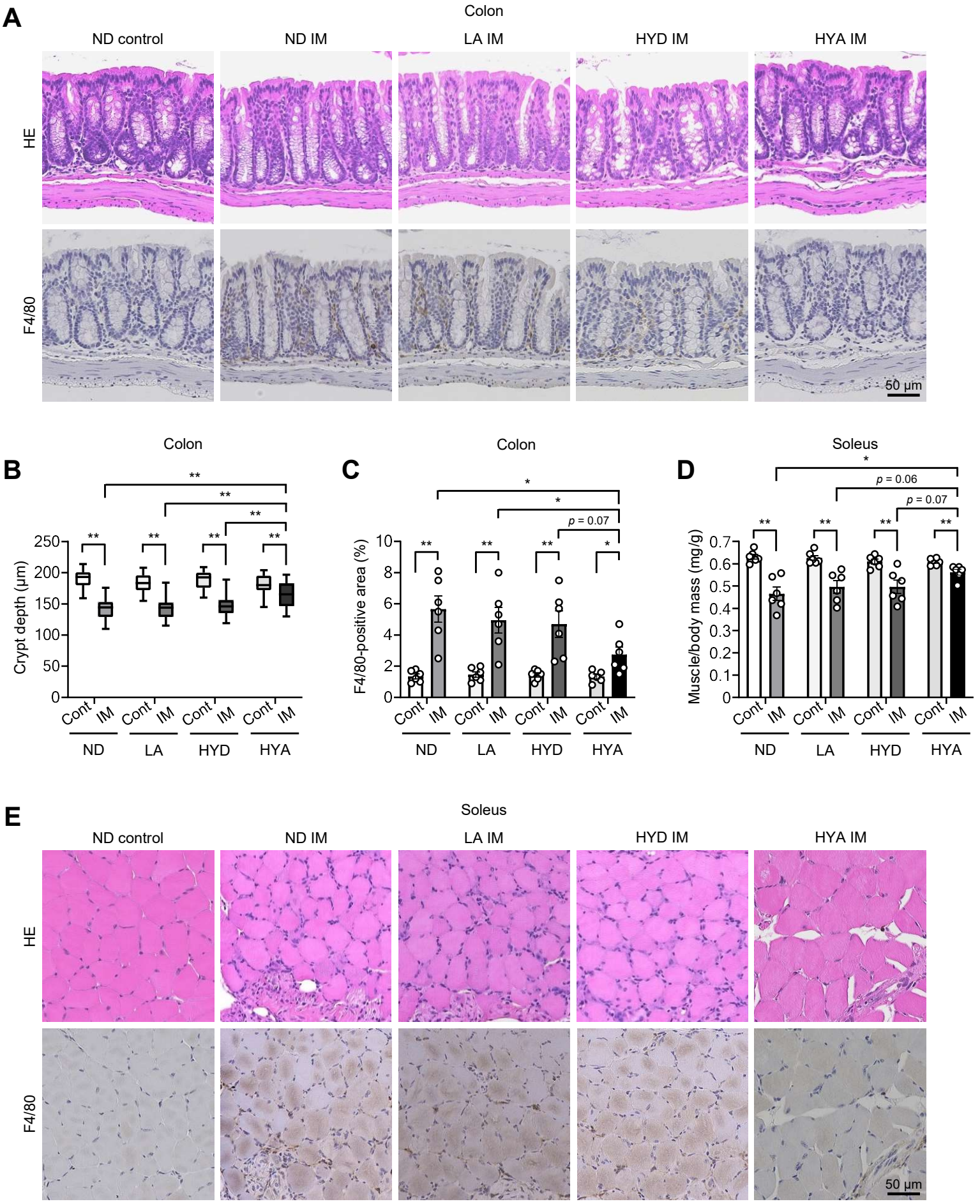
A
Colon
ND control
ND IM
LA IM
HYD IM
HYA IM
HE
F4/80
50 μm
B
Colon
Crypt depth (μm)
Cont
IM
ND
LA
HYD
HYA
C
Colon
F4/80-positive area (%)
p = 0.07
D
Soleus
Muscle/body mass (mg/g)
p = 0.06
p = 0.07
E
Soleus
ND control
ND IM
LA IM
HYD IM
HYA IM
HE
F4/80
50 μm

Figure 5. A gut microbial metabolite derived from LA inhibits intestinal and muscle inflammation as well as muscle atrophy induced by limb immobilization

(A–C) Hematoxylin-eosin and F4/80 immunohistochemical staining (A) for determination of crypt depth (B) and the F4/80-positive area (C) in the colon of mice fed a normal diet (ND) or a diet containing LA, HYD, or HYA and subjected (or not) to cast-fixation of the hind limbs for 10 days (n = 6 mice). The depth of 100 crypts pooled from four mice was measured and averaged for each condition in (B). Scale bar (A), 50 μm.

(D and E) Ratio of muscle mass to body mass (D) as well as hematoxylin-eosin and F4/80 immunohistochemical staining (E) for the soleus of mice (n = 6) treated as in (A) to (C). Scale bar (E), 50 μm.

Quantitative data are means ± SEM (C and D) or are presented as box-and-whisker plots (B). *$p < 0.05$, **$p < 0.01$ (two-way ANOVA with the Bonferroni post hoc test).

See also Figures S7 to S11.

Figure 6

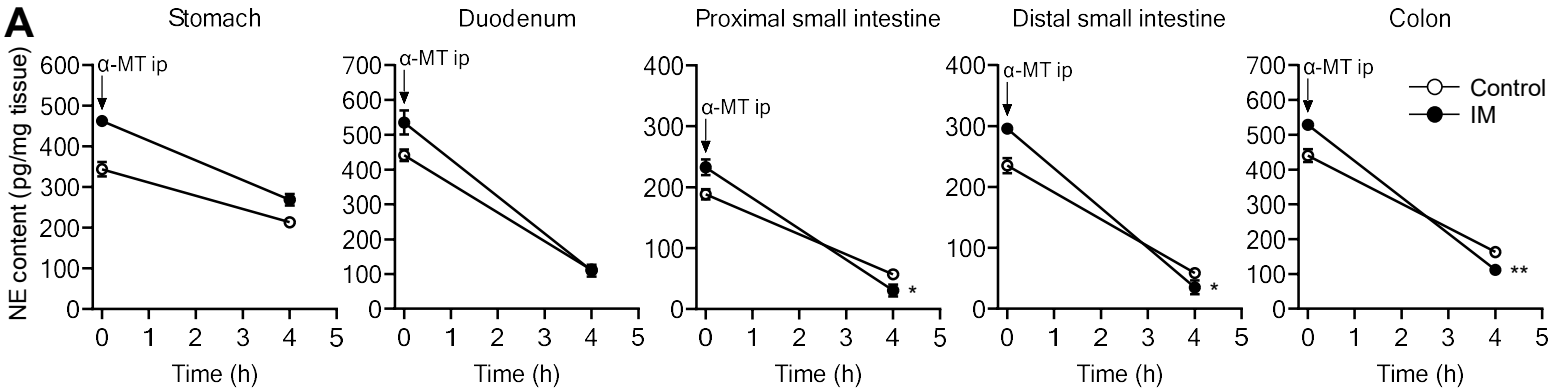
A
Stomach
Duodenum
Proximal small intestine
Distal small intestine
Colon
NE content (pg/mg tissue)
α-MT ip
Control
IM
Time (h)

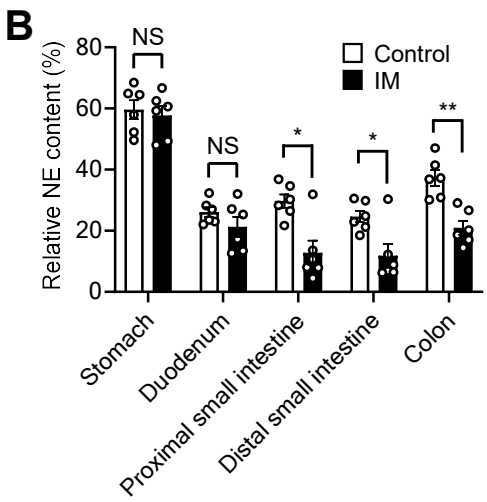
B
Relative NE content (%)
NS
Control
IM
Stomach
Duodenum
Proximal small intestine
Distal small intestine
Colon

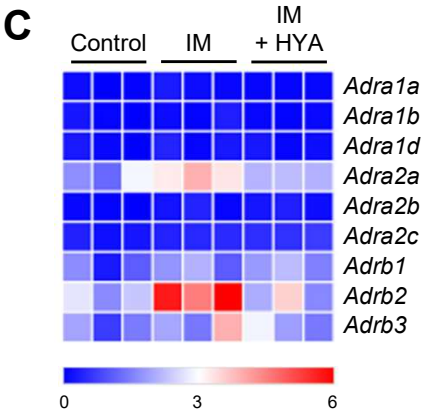
C
Control
IM
IM + HYA
Adra1a
Adra1b
Adra1d
Adra2a
Adra2b
Adra2c
Adrb1
Adrb2
Adrb3

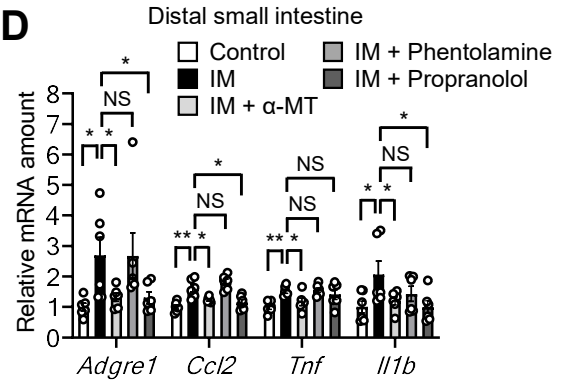
D
Distal small intestine
Control
IM
IM + α-MT
IM + Phentolamine
IM + Propranolol
Relative mRNA amount
NS
Adgre1
Ccl2
Tnf
Il1b

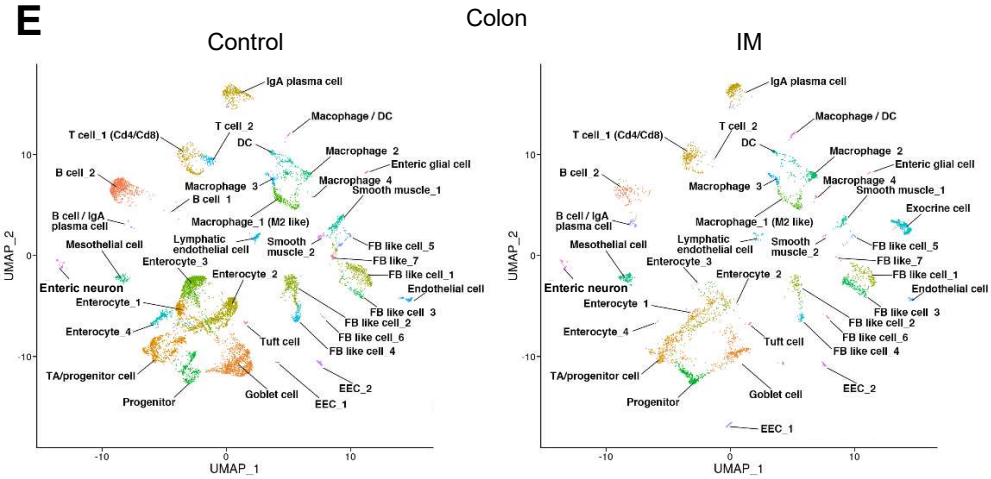
E
Colon
Control
IM
UMAP_1
UMAP_2

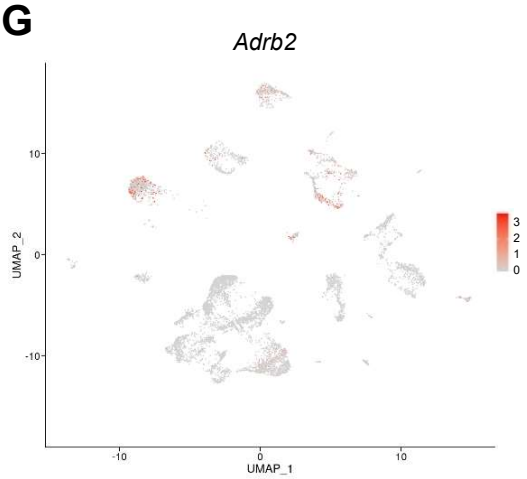
G
Adrb2
UMAP_1
UMAP_2

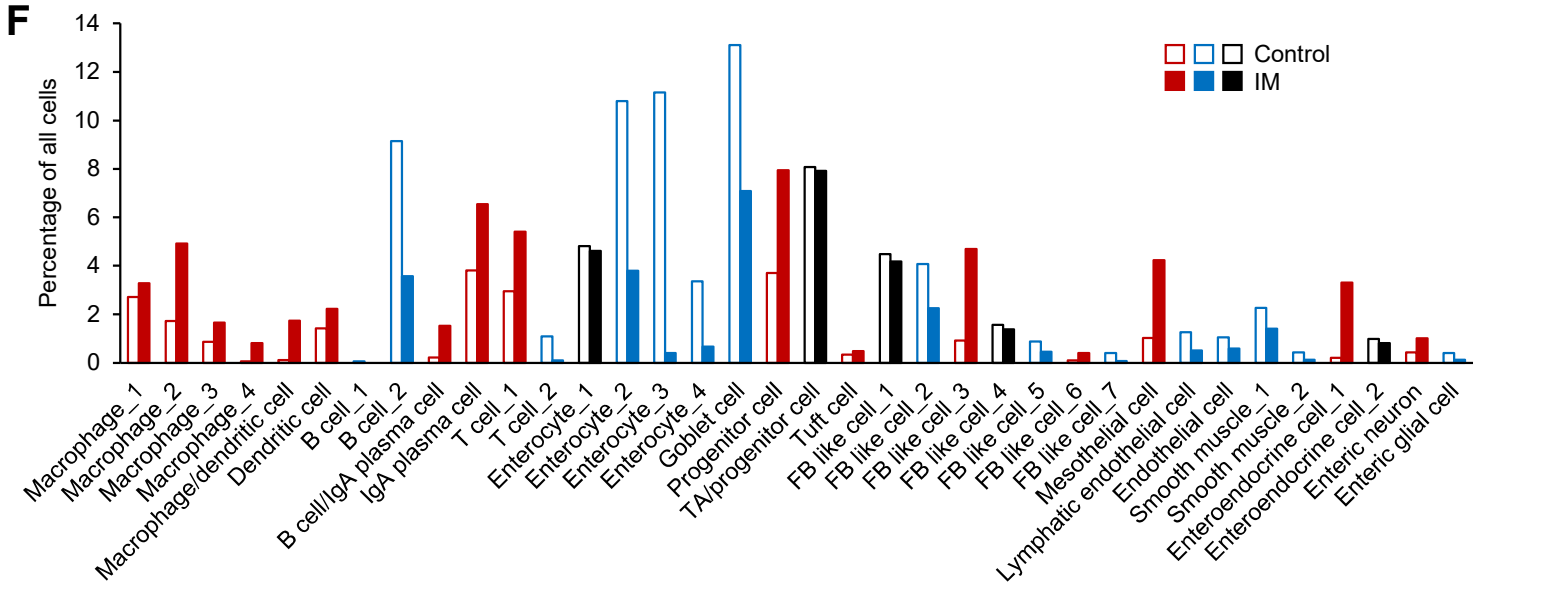
F
Percentage of all cells
Control
IM
Macrophage_1
Macrophage_2
Macrophage_3
Macrophage_4
Macrophage/dendritic cell
Dendritic cell
B cell_1
B cell_2
B cell/IgA plasma cell
IgA plasma cell
T cell_1
T cell_2
Enterocyte_1
Enterocyte_2
Enterocyte_3
Enterocyte_4
Goblet cell
Progenitor cell
TA/progenitor cell
Tuft cell
FB like cell_1
FB like cell_2
FB like cell_3
FB like cell_4
FB like cell_5
FB like cell_6
FB like cell_7
Mesothelial cell
Lymphatic endothelial cell
Endothelial cell
Smooth muscle_1
Smooth muscle_2
Enteroendocrine cell_1
Enteroendocrine cell_2
Enteric neuron
Enteric glial cell

Figure 6. Sympathetic nerve activation contributes to intestinal inflammation induced by limb immobilization

(A and B) NE content (A) and relative NE content (at 4 h versus 0 h) (B) for the stomach, duodenum, proximal and distal small intestine, and colon of control or cast-immobilized (10 days) mice at 0 and 4 h after intraperitoneal (ip) injection of α-MT (n = 6 mice).

(C) Heat map for the expression of adrenergic receptor genes in the colon of mice fed a normal diet or a diet containing HYA and subjected (or not) to cast-immobilization for 10 days (n = 3 mice).

(D) RT-qPCR analysis of inflammation-related gene expression in the distal small intestine of mice subjected to intraperitoneal injection of α-MT, phentolamine, propranolol, or vehicle daily for 10 days with or without concomitant cast-immobilization (n = 6 mice).

(E) Uniform manifold approximation and projection (UMAP) representation of 37 cell clusters identified by scRNA-seq analysis of the colon for control mice or mice subjected to cast-immobilization for 10 days. DC, dendritic cell; EEC, enteroendocrine cell; FB, fibroblast.

(F) Percentage of the indicated cell clusters among all cells. Red or blue squares indicate cell clusters for which cast-immobilization increased or decreased the cell ratio by >20%, respectively.

(G) Feature plot of *Adrb2* expression in the cell clusters of the colon.

Quantitative data in (A), (B), and (D) are means ± SEM. *$p < 0.05$, **$p < 0.01$, NS by the unpaired Student's t test (B) or two-way ANOVA with the Bonferroni post hoc test (A and D). See also Figures S12 and S13 as well as Table S1.

Figure 7

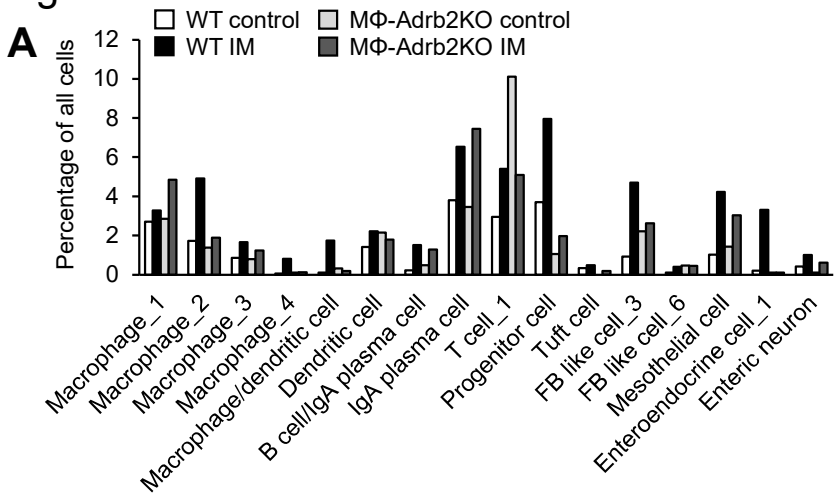
A
WT control
WT IM
MΦ-Adrb2KO control
MΦ-Adrb2KO IM
Percentage of all cells
Macrophage_1
Macrophage_2
Macrophage_3
Macrophage_4
Macrophage/dendritic cell
Dendritic cell
B cell/IgA plasma cell
IgA plasma cell
T cell_1
Progenitor cell
Tuft cell
FB like cell_3
FB like cell_6
Mesothelial cell
Enteroendocrine cell_1
Enteric neuron

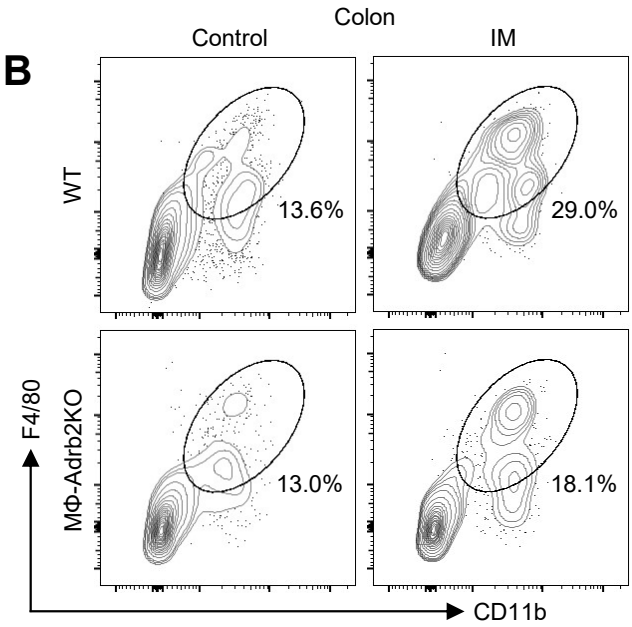
B
Colon
Control
IM
WT
MΦ-Adrb2KO
13.6%
29.0%
13.0%
18.1%
F4/80
CD11b

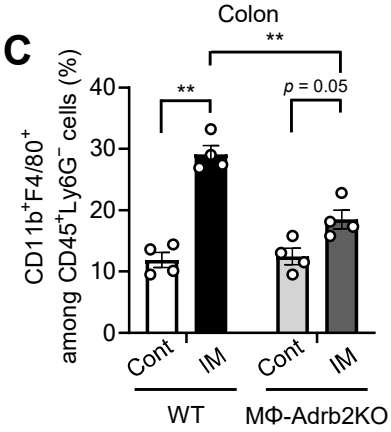
C
Colon
CD11b+F4/80+ among CD45+Ly6G− cells (%)
**
p = 0.05
Cont
IM
WT
MΦ-Adrb2KO

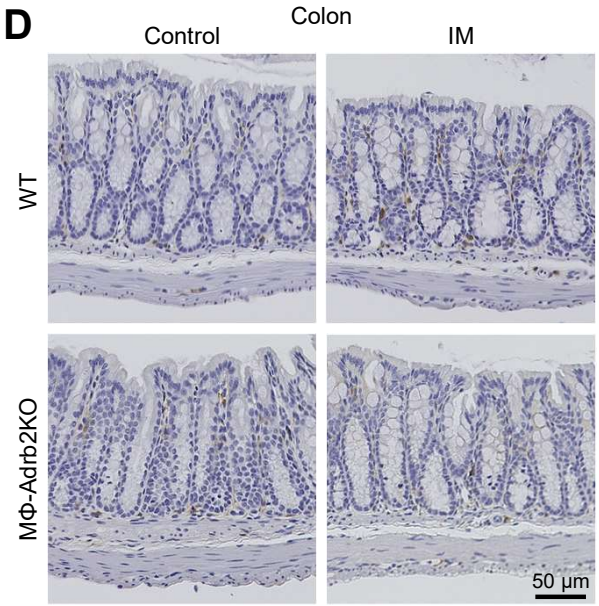
D
Colon
Control
IM
WT
MΦ-Adrb2KO
50 μm

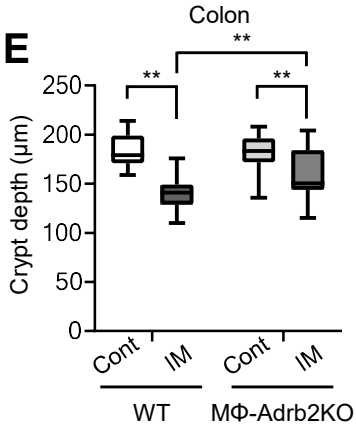
E
Colon
Crypt depth (μm)
**
Cont
IM
WT
MΦ-Adrb2KO

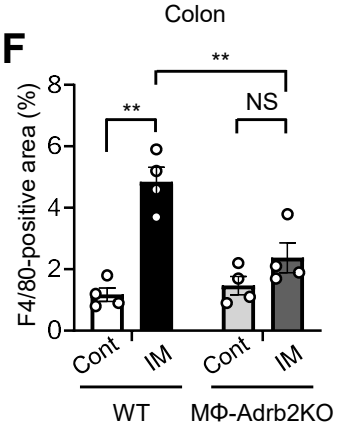
F
Colon
F4/80-positive area (%)
**
NS
Cont
IM
WT
MΦ-Adrb2KO

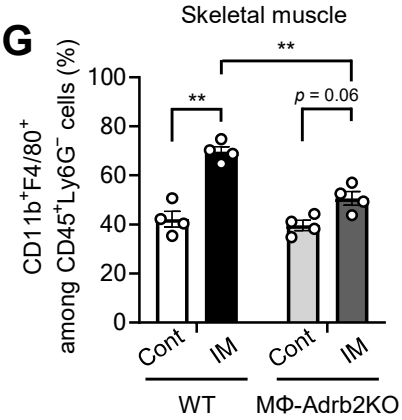
G
Skeletal muscle
CD11b+F4/80+ among CD45+Ly6G− cells (%)
**
p = 0.06
Cont
IM
WT
MΦ-Adrb2KO

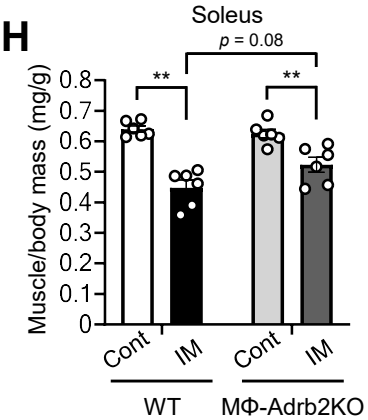
H
Soleus
Muscle/body mass (mg/g)
**
p = 0.08
Cont
IM
WT
MΦ-Adrb2KO

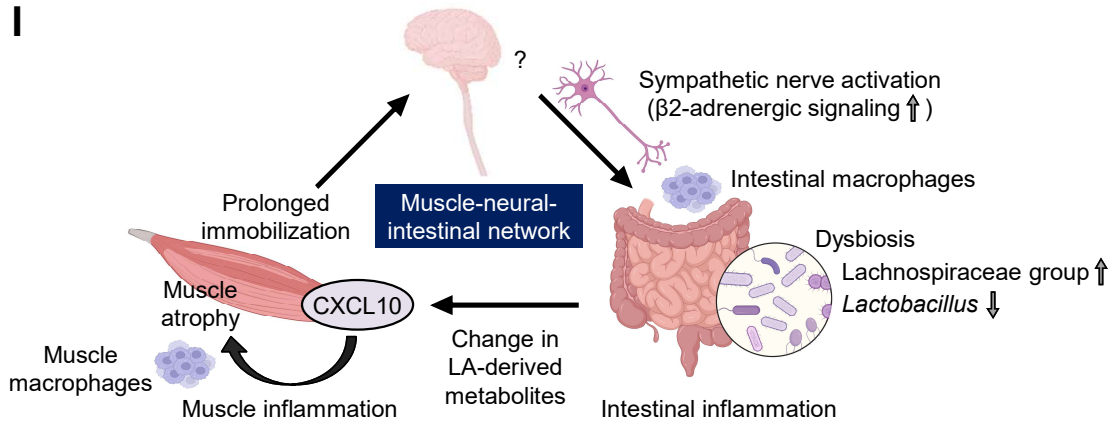
I
?
Sympathetic nerve activation
(β2-adrenergic signaling ⇑)
Intestinal macrophages
Prolonged immobilization
Muscle-neural-intestinal network
Dysbiosis
Lachnospiraceae group ⇑
Lactobacillus ⇓
Muscle atrophy
CXCL10
Muscle macrophages
Muscle inflammation
Change in LA-derived metabolites
Intestinal inflammation

Figure 7. Prevention of β2-adrenergic signaling in macrophages attenuates intestinal and muscle inflammation induced by prolonged limb immobilization

(A–H) Percentage of the indicated cell clusters among all cells in the colon as determined by scRNA-seq analysis (A); representative flow cytometric analysis (B) and the percentage (*n* = 4 mice) (C) of $CD11b^{+}F4/80^{+}$ cells among $CD45^{+}Ly6G^{-}$ cells in the colon; F4/80 immunohistochemical staining of the colon (D) for determination of crypt depth (*n* = 4 mice) (E) and the F4/80-positive area (*n* = 4 mice) (F); the percentage of $CD11b^{+}F4/80^{+}$ cells among $CD45^{+}Ly6G^{-}$ cells in hind limb skeletal muscle (*n* = 4 mice) (G); and the ratio of soleus muscle mass to body mass (*n* = 6 mice) (H) for wild-type (WT) or macrophage-specific Adrb2 KO (MΦ-Adrb2KO) mice subjected (or not) to cast-immobilization for 10 days. The depth of 100 crypts pooled from four mice was measured and averaged for each condition in (E). Scale bar (D), 50 μm. Quantitative data are means ± SEM (C and F–H) or are presented as box-and-whisker plots (E). $^{**}p < 0.01$, NS (two-way ANOVA with the Bonferroni post hoc test).

(I) Proposed role of a skeletal muscle–sympathetic nerve–intestine network in immobilization-induced muscle inflammation and atrophy.

See also Figures S14 and Table S1.

Supplemental Figure 1

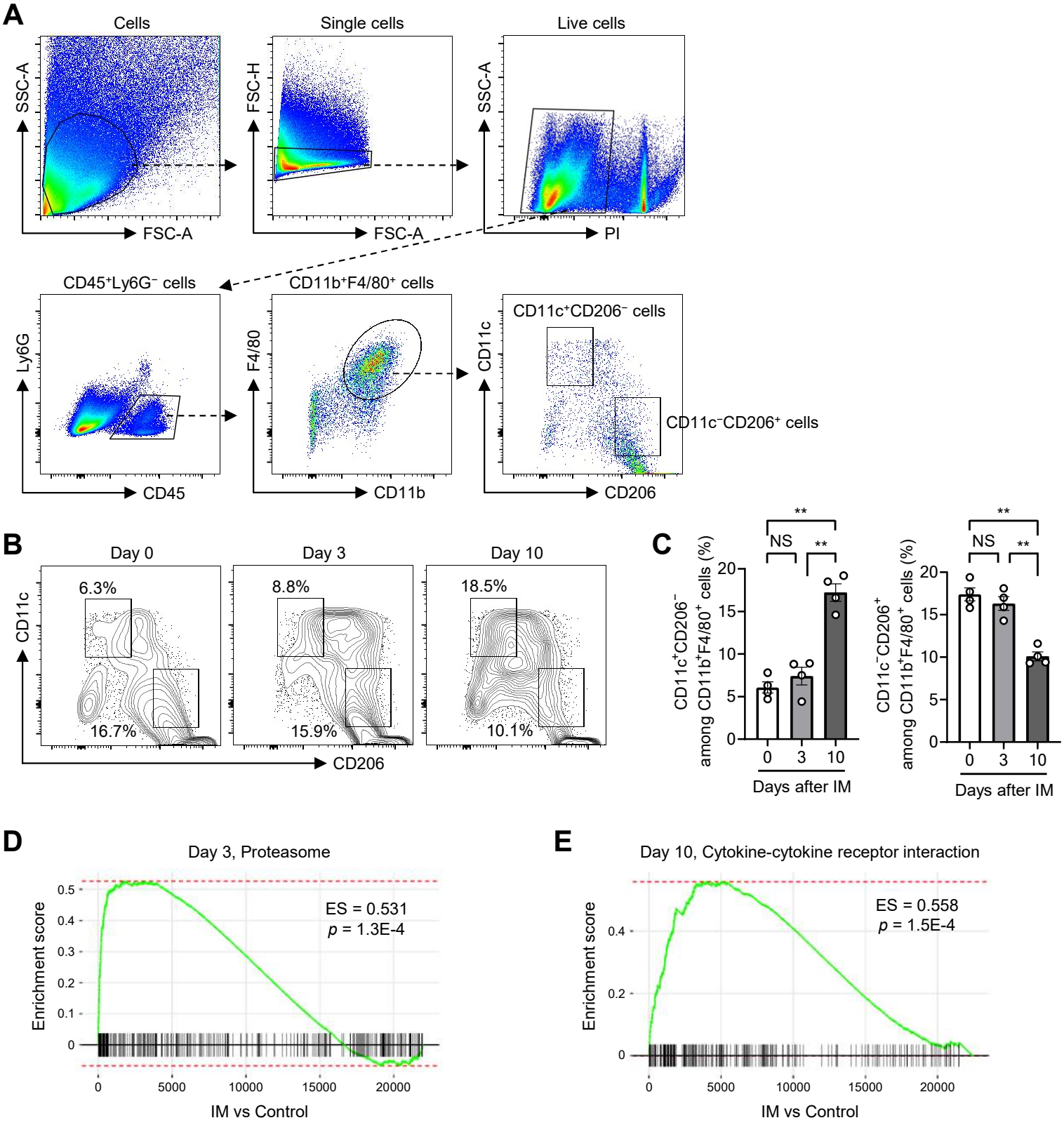

Figure S1, related to Figure 1. Gating strategy and immobilization-induced changes in macrophage subsets of skeletal muscle as well as GSEA for immobilized muscle

(A) Gating strategy for fluorescence-activated sorting of macrophages from skeletal muscle of immobilized mice. SSC, side scatter; FSC, forward scatter; PI, propidium iodide.

(B and C) Representative flow cytometric analysis (B) and the percentage (C) of $CD11c^{+}CD206^{-}$ or $CD11c^{-}CD206^{+}$ cells in skeletal muscle of mice subjected to hind limb immobilization by cast-fixation for the indicated times (n = 4 mice). Data in (C) are means ± SEM. $^{**}p < 0.01$, NS (two-way ANOVA with the Bonferroni post hoc test).

(D and E) GSEA for the indicated pathways performed with RNA-seq data from gastrocnemius muscle of mice immobilized for 3 days (D) or 10 days (E). ES, enrichment score.

Supplemental Figure 2

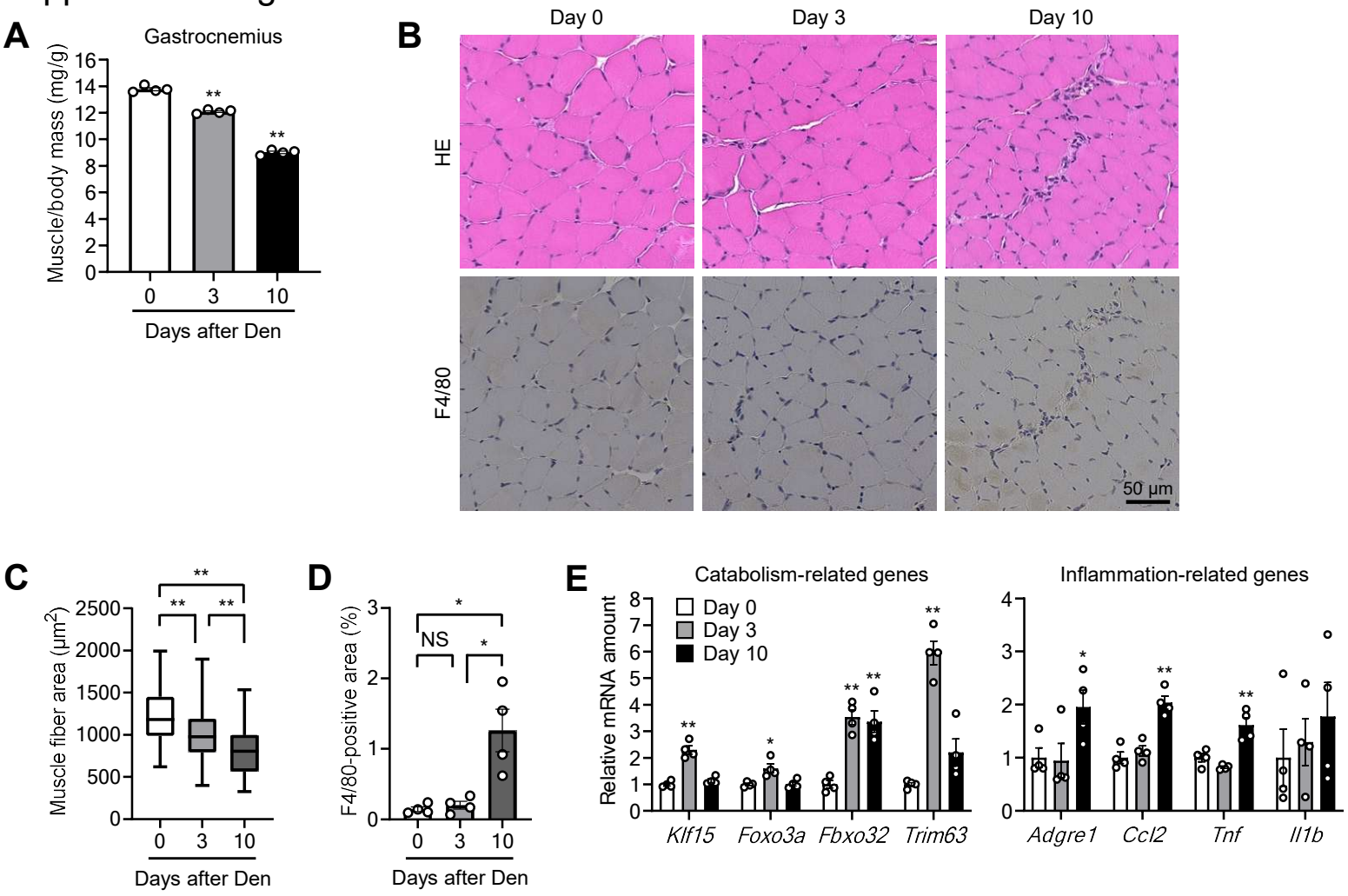

Figure S2, related to Figure 1. Time course of denervation-induced muscle atrophy, macrophage accumulation, and changes in gene expression

(A) Ratio of gastrocnemius muscle mass in both hind limbs to body mass for mice subjected to bilateral hind limb denervation (Den) for the indicated times (n = 4 mice). (B–D) Hematoxylin-eosin and F4/80 immunohistochemical staining (B) for determination of muscle fiber area (C) and the F4/80-positive area (D) in soleus muscle of denervated mice (n = 4 mice). The area of 800 fibers pooled from four mice was measured and averaged for each condition in (C). Scale bar (B), 50 μm.

(E) RT-qPCR analysis of protein catabolism– or inflammation-related gene expression in the gastrocnemius of denervated mice (n = 4 mice).

Quantitative data are presented as means ± SEM (A, D, and E) or as box-and-whisker plots (C). *$p < 0.05$, **$p < 0.01$, NS (two-way ANOVA with the Bonferroni post hoc test) versus day 0 (A and E) or as indicated (C and D).

Supplemental Figure 3

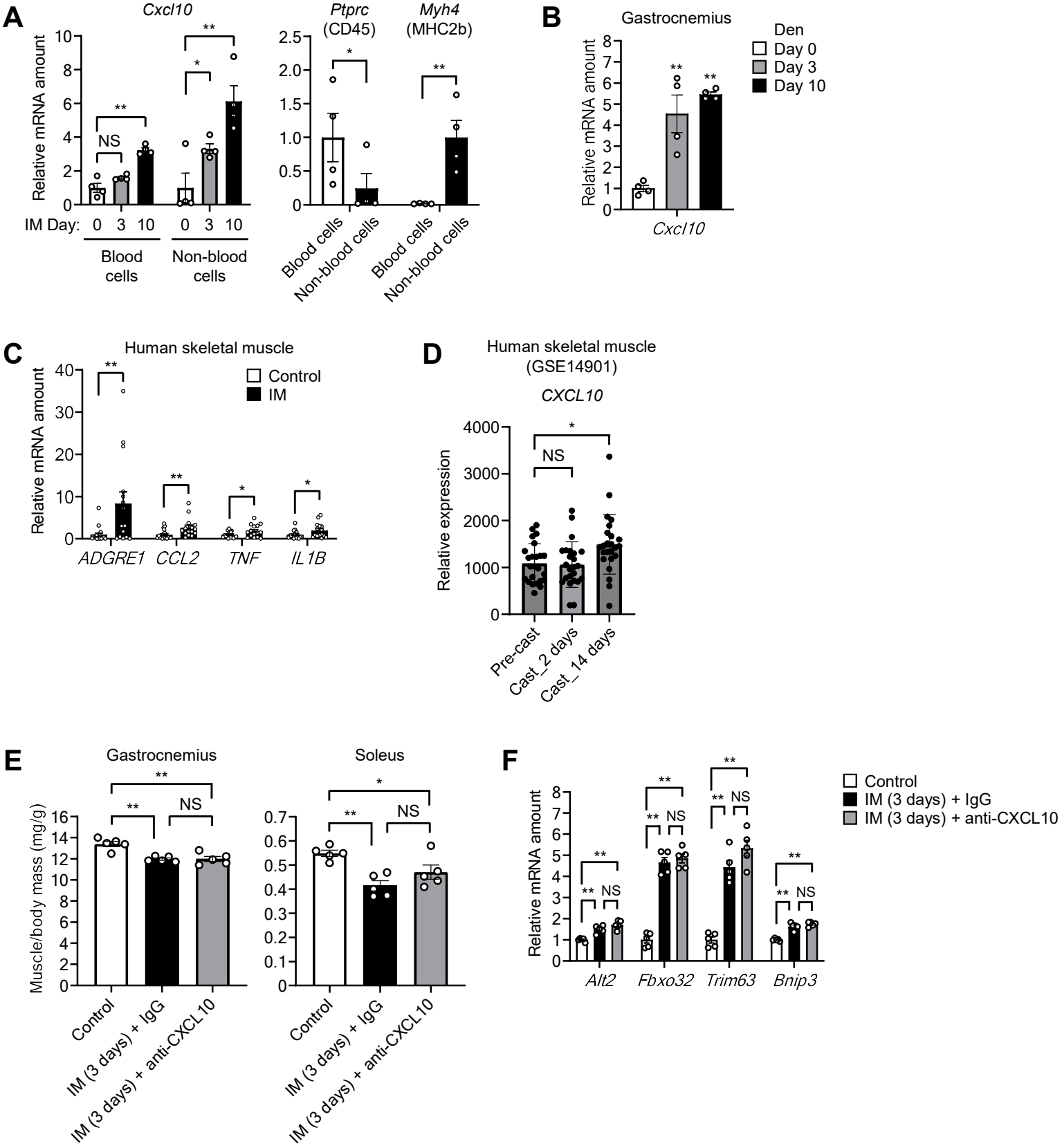

Figure S3, related to Figure 2. Identification of the chemokine CXCL10 as a mediator of muscle inflammation induced by limb immobilization

(A) RT-qPCR analysis of *Cxcl10*, *Ptprc*, and *Myh4* mRNA abundance in the blood cell and non–blood cell fractions of skeletal muscle from cast-immobilized mice (n = 4 mice).

(B) RT-qPCR analysis of *Cxcl10* mRNA in gastrocnemius of denervated mice (n = 4 mice).

(C) RT-qPCR analysis of inflammation-related gene expression in skeletal muscle of control (n = 18) or immobilized (n = 15) human participants.

(D) Relative expression of *CXCL10* in skeletal muscle of healthy human individuals subjected to cast-immobilization as determined from a publicly available data set. The relative expression level is presented as transcripts per million (TPM) for the subjects before (Pre-cast) and at two time points after (Cast_2 days and Cast_14 days) cast application. Each point represents one individual.

(E and F) Ratio of muscle mass to body mass (E) and RT-qPCR analysis of catabolism-related gene expression in gastrocnemius (F) for control mice or mice subjected to intraperitoneal injection of neutralizing antibodies to CXCL10 (0.1 mg/body) or of control IgG at 3 days before cast-immobilization for 3 days (n = 5 mice).

All data are means ± SEM. *$p < 0.05$, **$p < 0.01$, NS compared with day 0 (B) or as indicated (A and C–F) by the unpaired Student's t test (A and C), two-way ANOVA with the Bonferroni post hoc test (A, B, E, and F), or one-way ANOVA followed by Dunnett's test (D).

Supplemental Figure 4

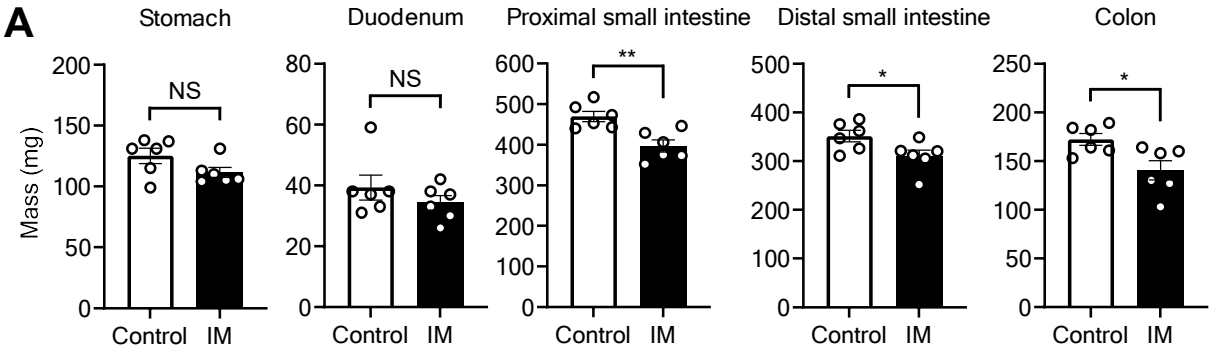

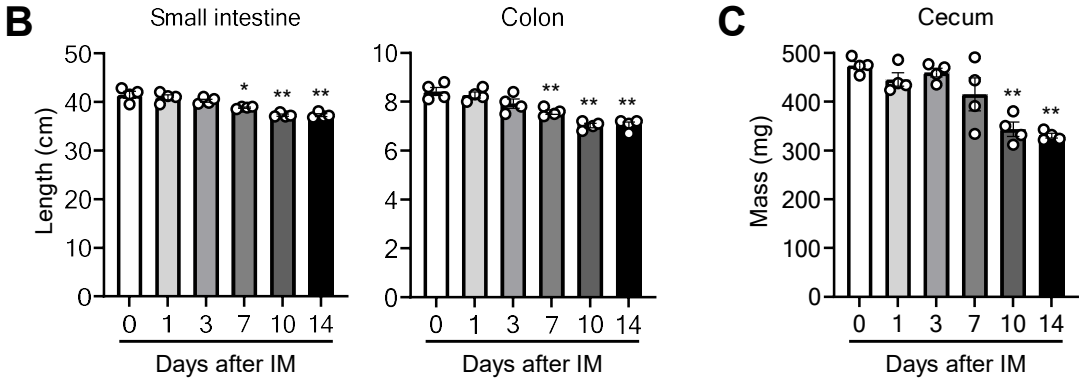

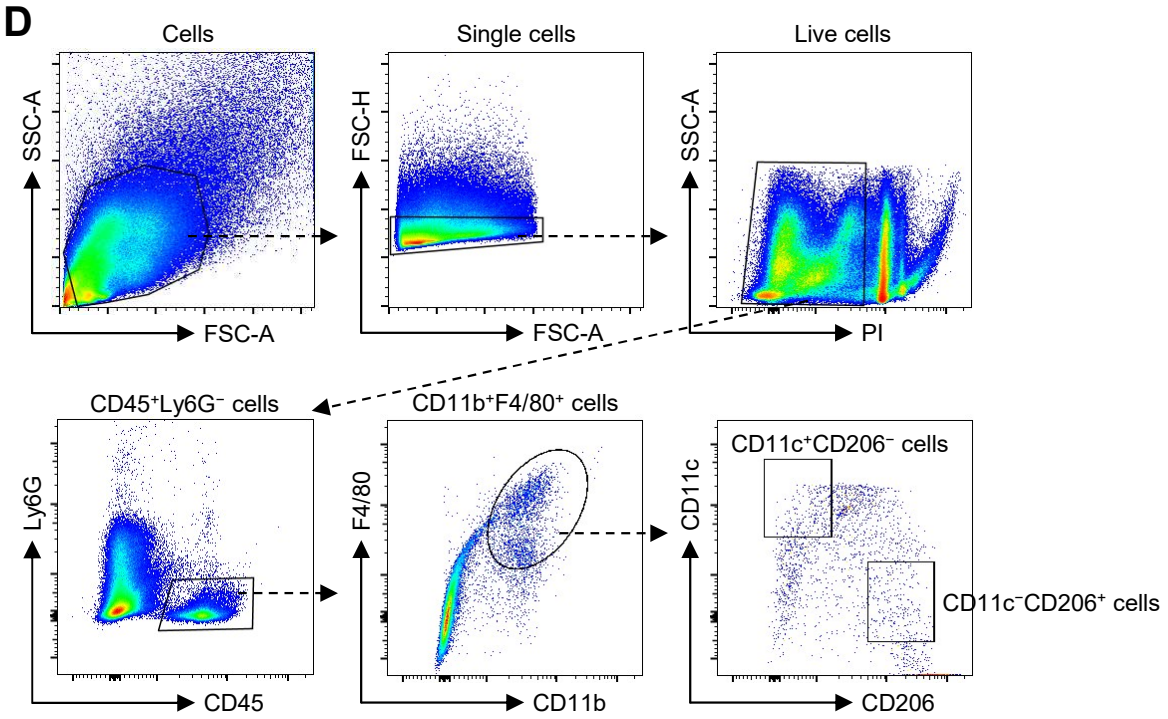

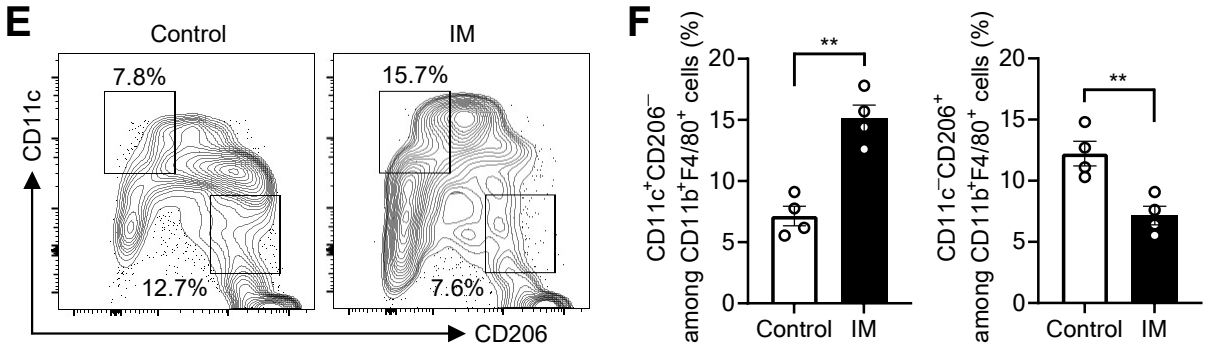

Figure S4, related to Figure 3. Effects of prolonged limb immobilization on intestinal tissue, and gating strategy for macrophage subsets in the colon

(A) Mass of the stomach, duodenum, proximal and distal small intestine, and colon for control mice or mice subjected to cast-immobilization for 10 days (n = 6 mice).

(B and C) Length of the small intestine and colon (B) as well as mass of the cecum (C) for mice subjected to cast-immobilization for the indicated times (n = 4 mice).

(D) Gating strategy for fluorescence-activated sorting of macrophages from the colon of immobilized mice.

(E and F) Representative flow cytometric analysis (E) and the percentage (F) of $CD11c^{+}CD206^{-}$ cells and $CD11c^{-}CD206^{+}$ cells in the colon of cast-immobilized (10 days) and control mice (n = 4 mice).

Quantitative data are means ± SEM. *$p < 0.05$, **$p < 0.01$, NS compared with day 0 (B and C) or as indicated (A and F) by the unpaired Student's t test (A and F) or two-way ANOVA with the Bonferroni post hoc test (B and C).

Supplemental Figure 5

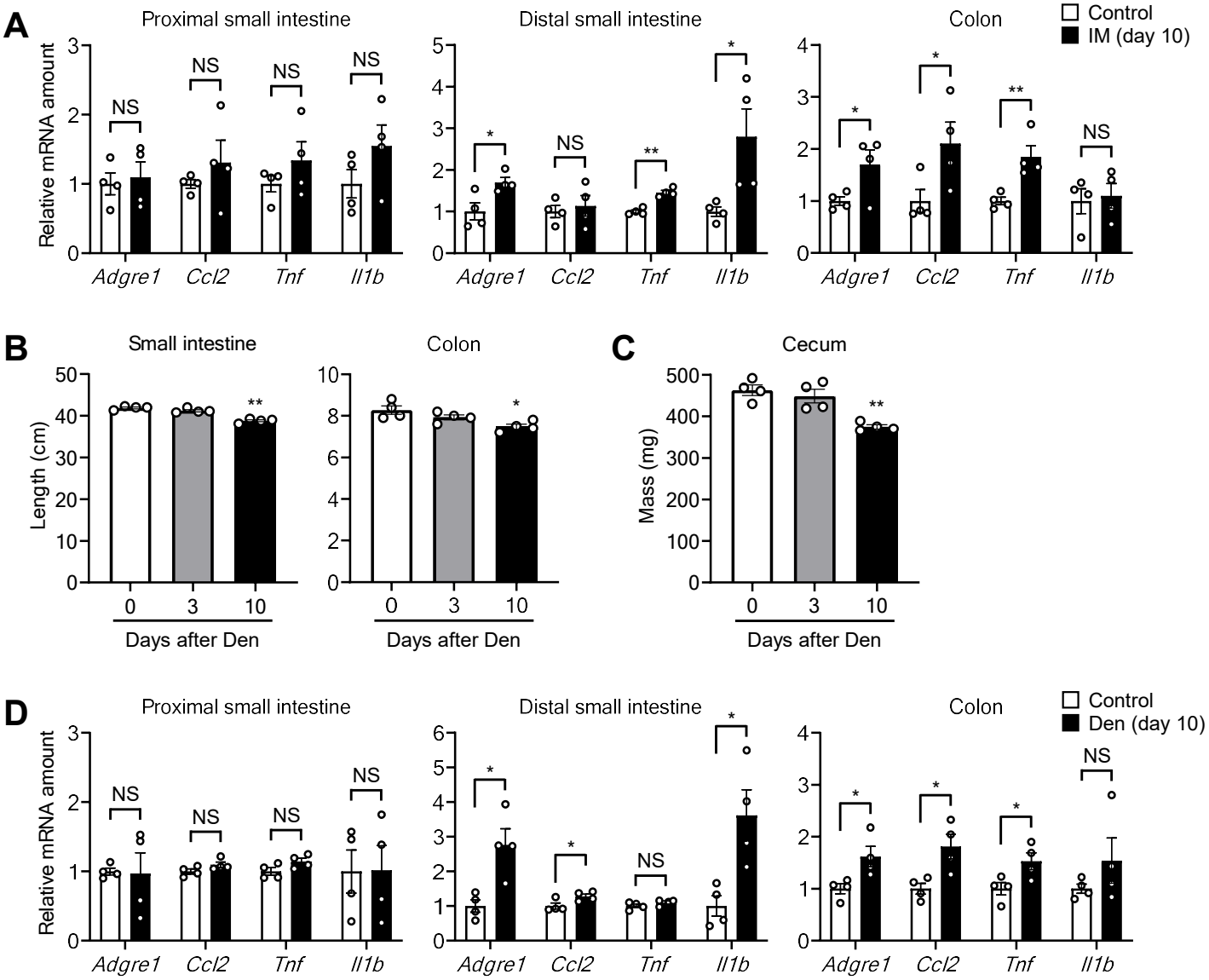

Figure S5, related to Figure 3. Effects of prolonged limb immobilization by cast-fixation or denervation on intestinal tissue

(A) RT-qPCR analysis of inflammation-related gene expression in the proximal or distal small intestine and colon of cast-immobilized (10 days) and control mice (n = 4 mice).

(B and C) Length of the small intestine and colon (B) as well as mass of the cecum (C) for mice subjected to limb denervation for the indicated times (n = 4 mice).

(D) RT-qPCR analysis of inflammation-related gene expression in the proximal or distal small intestine and colon of denervated and control mice (n = 4 mice).

All data are means ± SEM. *$p < 0.05$, **$p < 0.01$, NS compared with day 0 (B and C) or as indicated (A and D) by the unpaired Student's t test (A and D) or two-way ANOVA with the Bonferroni post hoc test (B and C).

Supplemental Figure 6

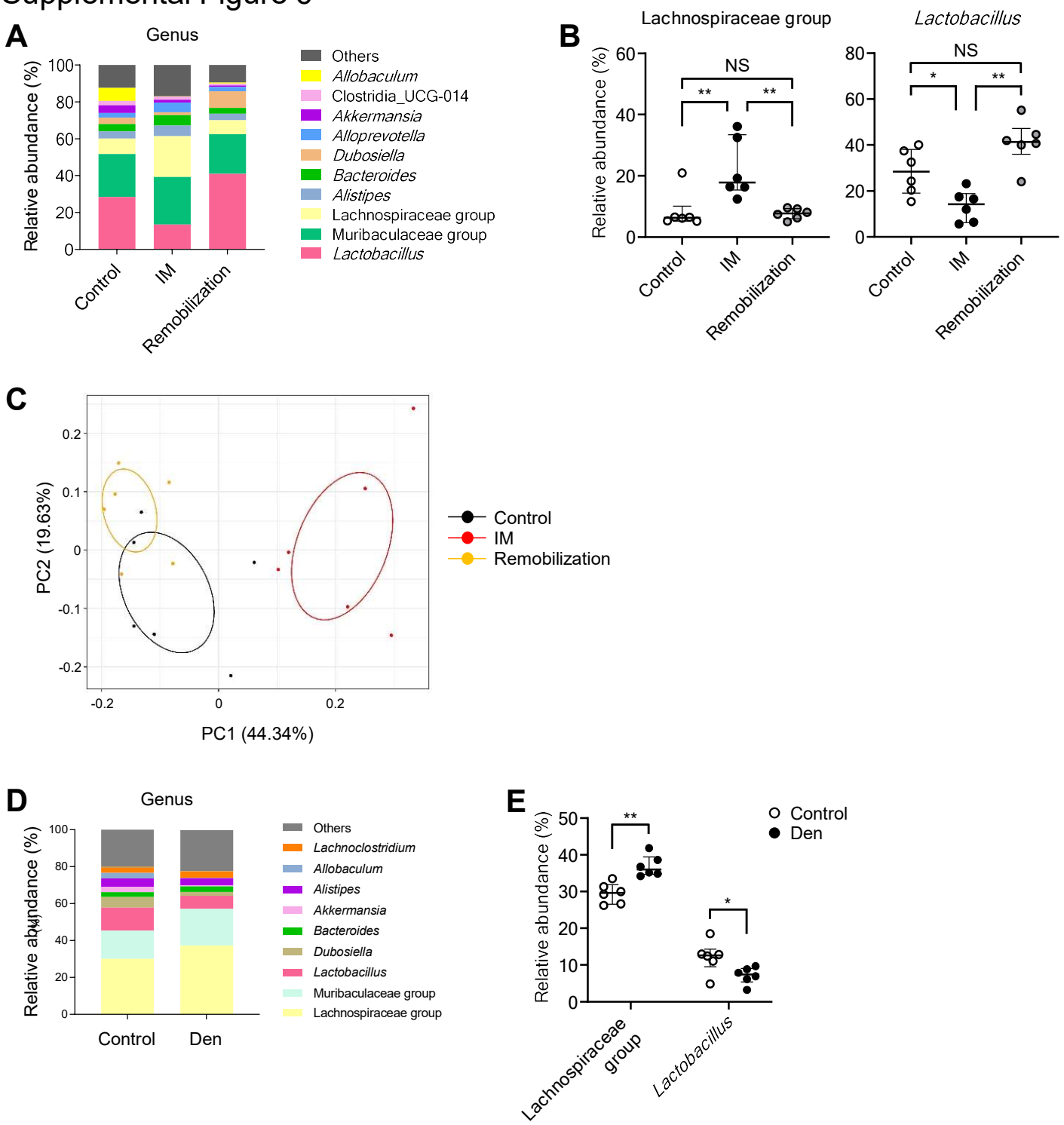

Figure S6, related to Figure 4. Effects of prolonged limb immobilization by cast-fixation or denervation on the gut microbiota

(A–C) Gut microbial composition at the genus level (A), relative abundance of the Lachnospiraceae group and *Lactobacillus* species (B), and corresponding principal component analysis (C) for control mice and mice subjected to cast immobilization for 10 days with (remobilization) or without subsequent cast removal for 14 days (n = 6 mice).
(D and E) Gut microbial composition at the genus level (D) and relative abundance of the Lachnospiraceae group and *Lactobacillus* species (E) for control mice or mice subjected to hind limb denervation for 10 days (n = 6 mice).
Quantitative data in (B) and (E) are presented as the median and interquartile range. *$p < 0.05$, **$p < 0.01$, NS by one-way ANOVA with the Bonferroni post hoc test (B) or the Mann-Whitney U test (E).

Supplemental Figure 7

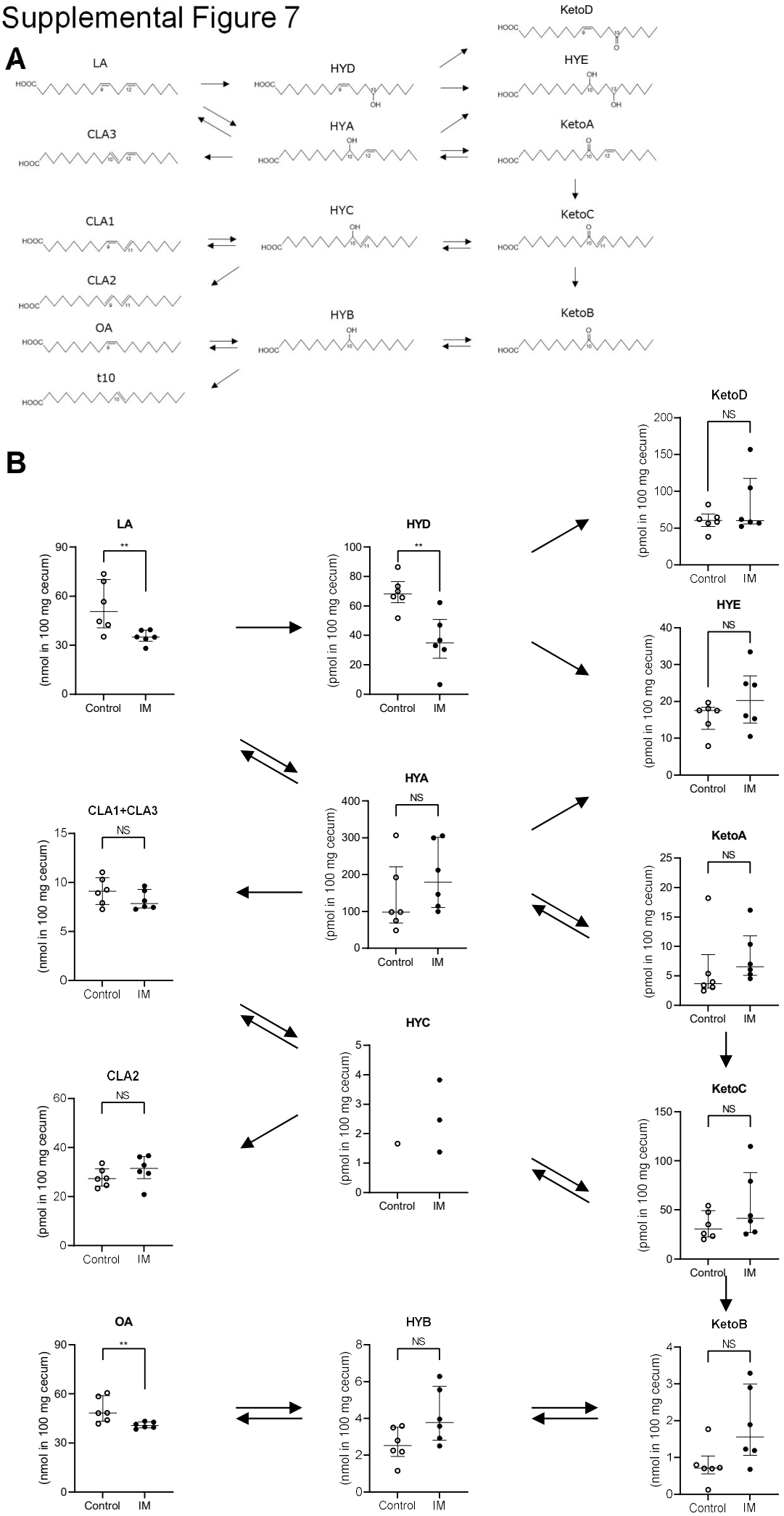

Figure S7, related to Figure 5. Prolonged limb immobilization by cast-fixation influences the fecal levels of fatty acid metabolites produced by the gut microbiota

(A) Metabolic pathway of LA showing the structure of fatty acid metabolites.

(B) Fatty acid concentrations in cecal content of mice subjected (or not) to cast-immobilization for 10 days (n = 6 mice). HYC was below the detection limit in most samples. Data are medians with the interquartile range. $^{**}p < 0.01$, NS (Mann-Whitney U test).

Supplemental Figure 8

A

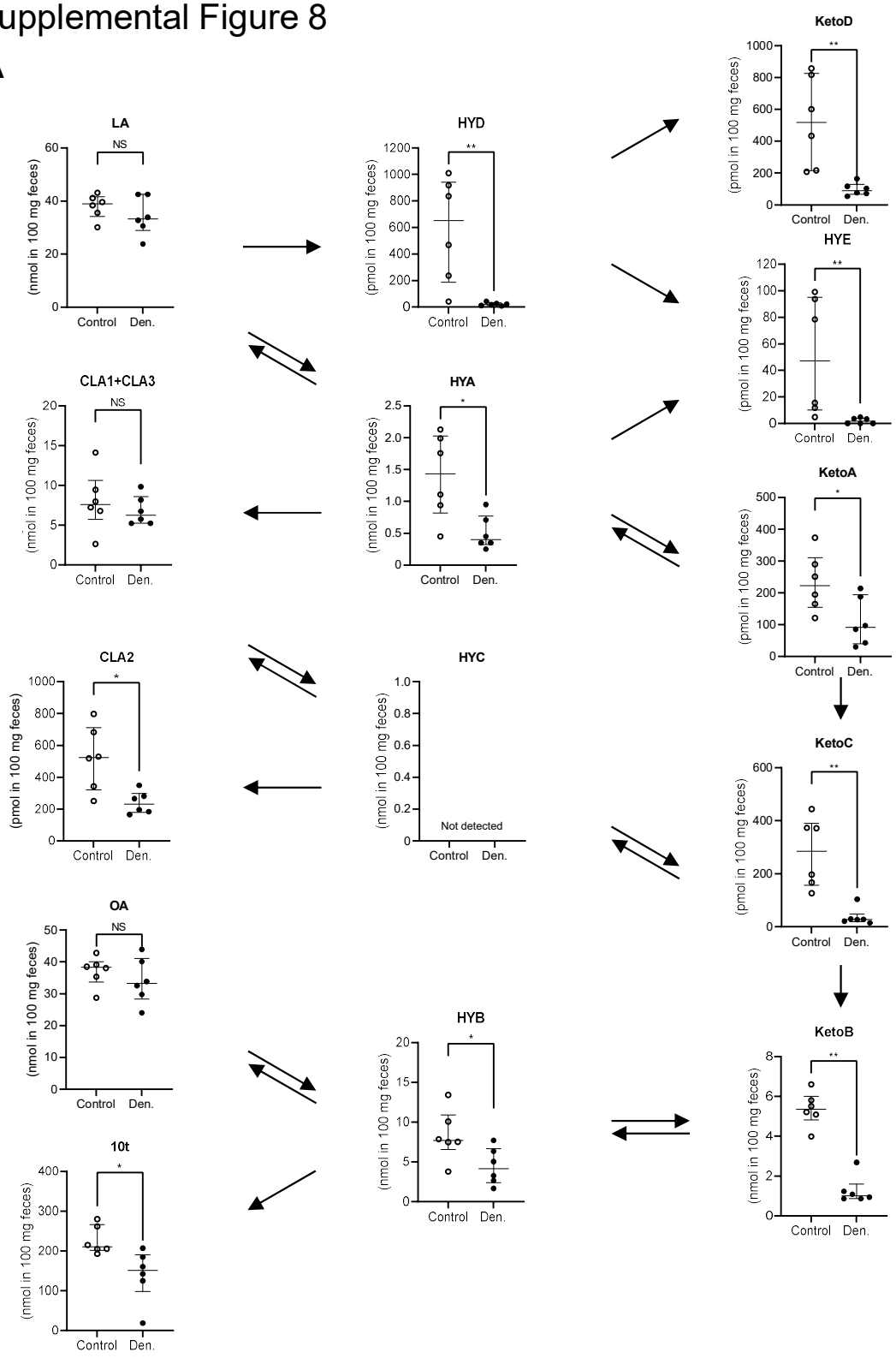

B

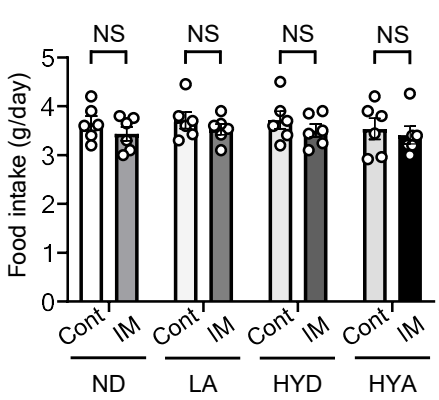

Figure S8, related to Figure 5. Prolonged limb immobilization by denervation influences the fecal levels of fatty acid metabolites produced by the gut microbiota (A) Fatty acid concentrations in feces of control and denervated mice (10 days) (n = 6 mice). HYC was below the detection limit in all samples.
(B) Daily food intake of mice maintained on a normal diet (ND) or a diet containing LA, HYD, or HYA and subjected (or not) to cast-immobilization for 10 days (n = 6 mice).
Data are medians with the interquartile range (A) or means ± SEM (B). *$p < 0.05$, **$p < 0.01$, NS by the Mann-Whitney U test (A) or two-way ANOVA with the Bonferroni post hoc test (B).

Supplemental Figure 9

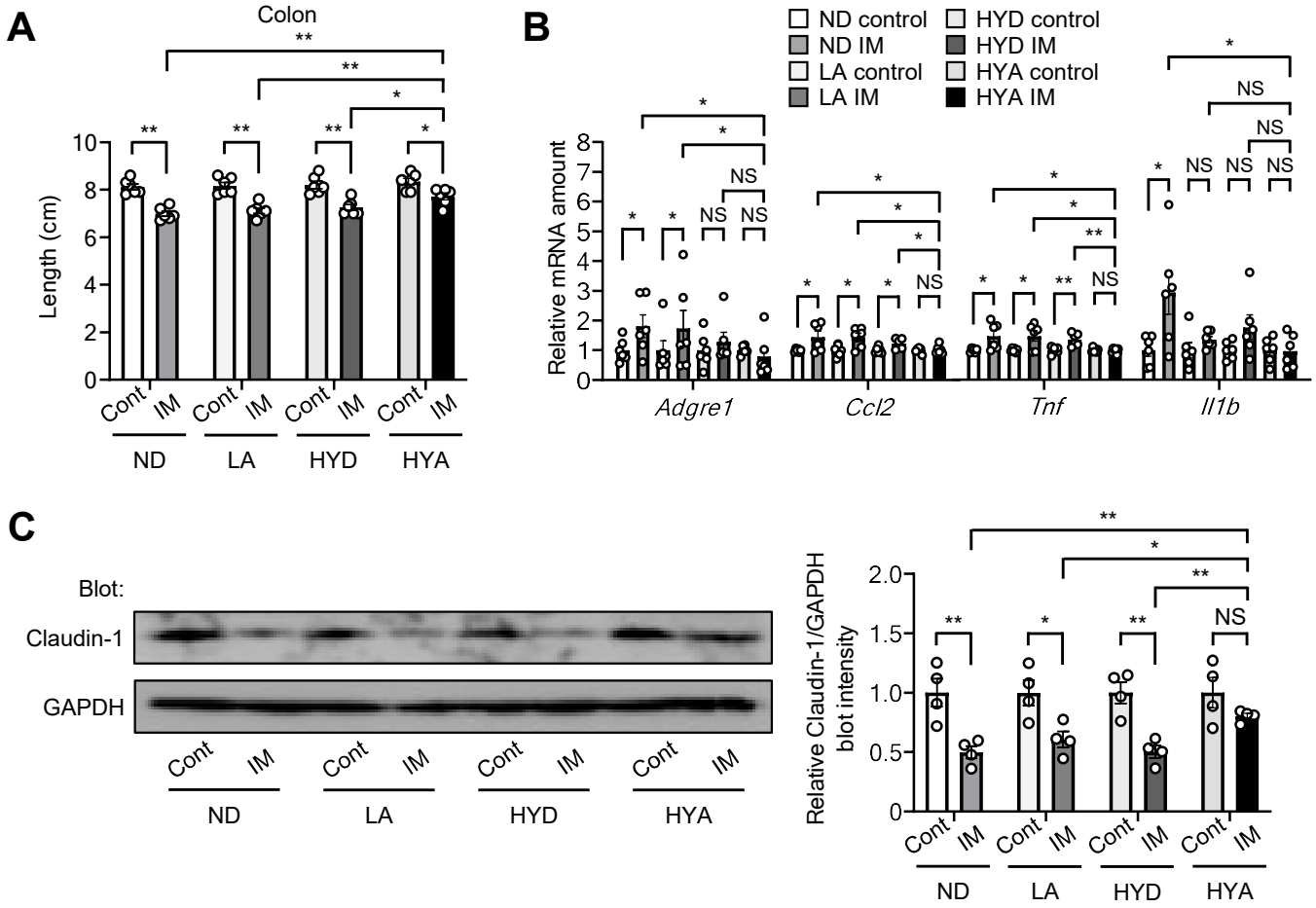

Figure S9, related to Figure 5. Effects of HYA on intestinal inflammation induced by prolonged limb immobilization

(A–C) Length of the colon (*n* = 6 mice) (A), RT-qPCR analysis of inflammation-related gene expression in the colon (*n* = 6 mice) (B), and immunoblot analysis of claudin-1 in the colon (*n* = 4 mice) (C) of mice fed a normal diet or a diet containing LA, HYD, or HYA and subjected (or not) to cast-immobilization for 10 days.

All quantitative data are means ± SEM. *$p < 0.05$, **$p < 0.01$, NS (two-way ANOVA with the Bonferroni post hoc test).

See also Figure S15.

Supplemental Figure 10

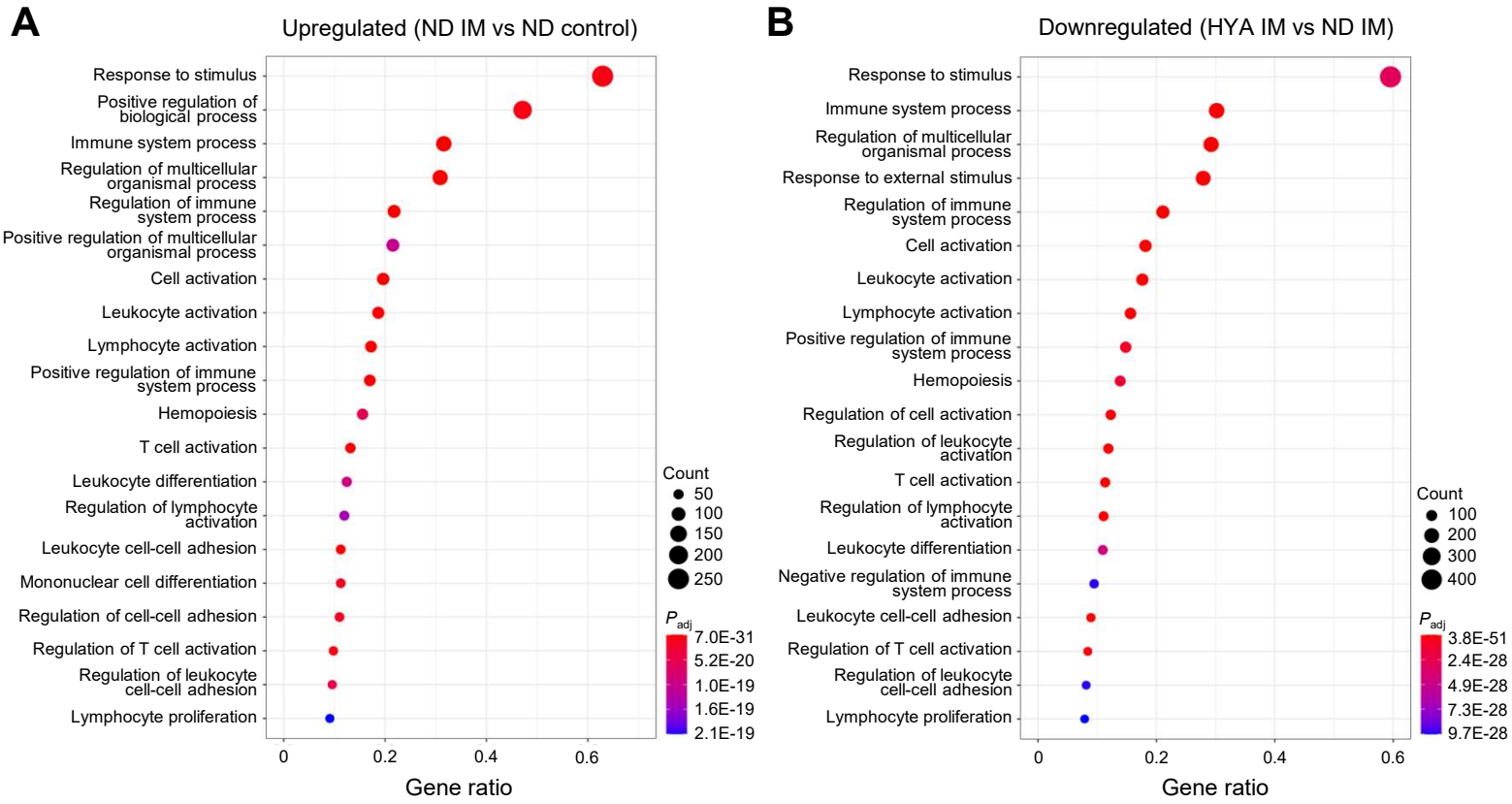

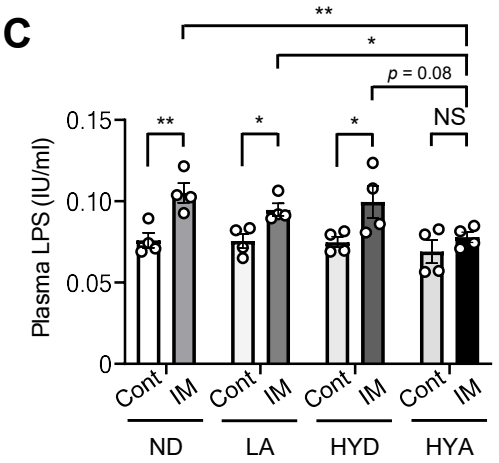

Figure S10, related to Figure 5. Effects of HYA on intestinal inflammation induced by prolonged limb immobilization

(A and B) GO functional analysis of RNA-seq data from the colon for biological processes upregulated in mice fed a normal diet and subjected to cast-immobilization for 10 days versus those not subjected to immobilization (A) as well as for biological processes downregulated in immobilized mice fed a diet containing HYA versus those fed a normal diet (B). The top 20 processes enriched among genes whose expression was altered by each condition are shown. p_{adj}, adjusted p value.

(C) Plasma concentration of LPS in mice fed a normal diet or a diet containing LA, HYD, or HYA and subjected (or not) to cast-immobilization for 10 days (n = 4 mice). Data are means ± SEM. *$p < 0.05$, **$p < 0.01$, NS (two-way ANOVA with the Bonferroni post hoc test).

Supplemental Figure 11

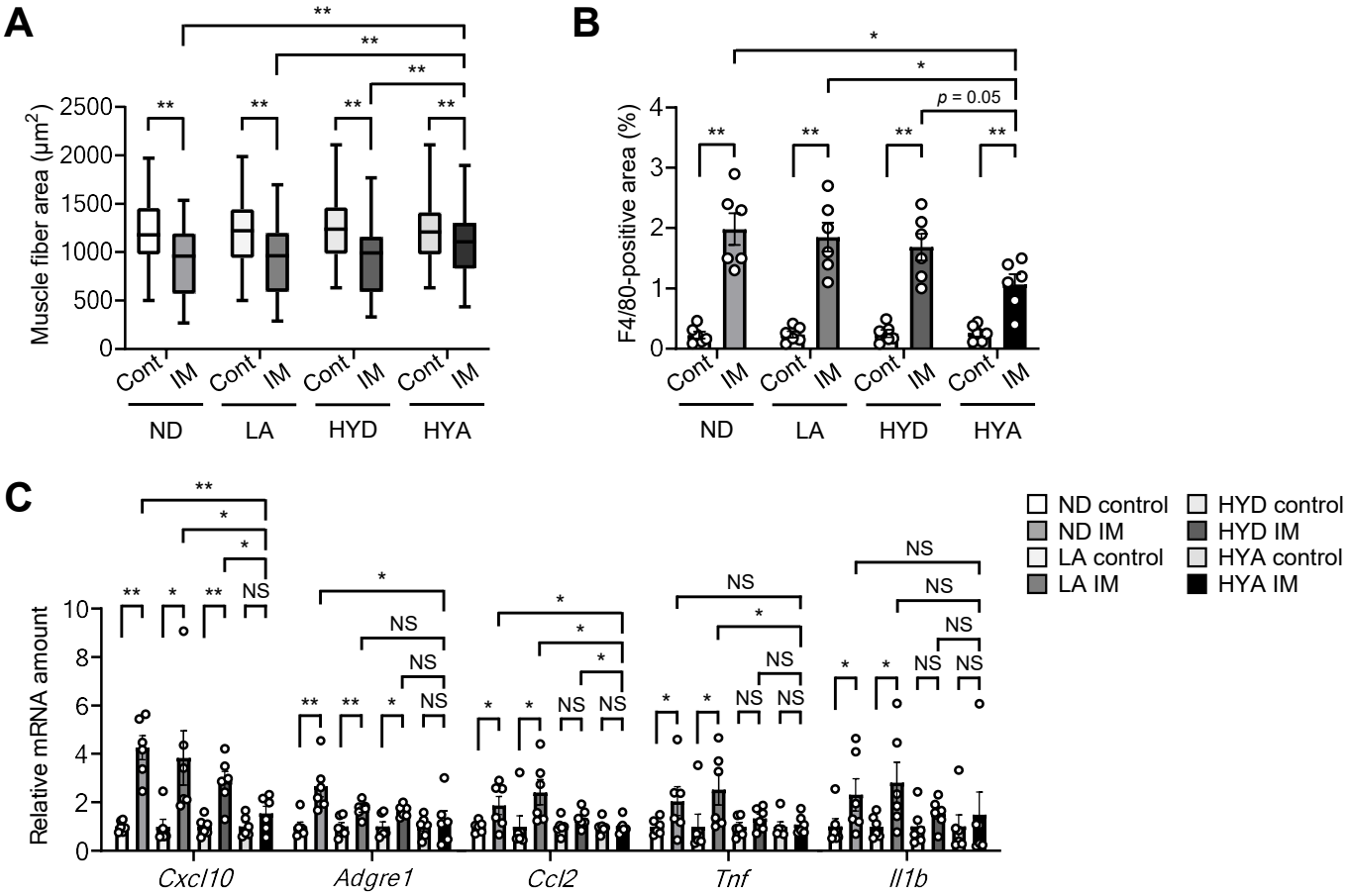

Figure S11, related to Figure 5. Effects of HYA on muscle inflammation and atrophy induced by prolonged limb immobilization

(A–C) Muscle fiber area (A) and the F4/80-positive area (B) in soleus (determined from images as in Figure 5E) as well as RT-qPCR analysis of inflammation-related gene expression in gastrocnemius (C) for mice fed a normal diet or a diet supplemented with LA, HYD, or HYA and subjected (or not) to cast-immobilization for 10 days (n = 6 mice). The area of 400 fibers pooled from four mice was measured and averaged for each condition in (A). Data are presented as box-and-whisker plots (A) or are means ± SEM (B and C). *$p < 0.05$, **$p < 0.01$, NS (two-way ANOVA with the Bonferroni post hoc test).

Supplemental Figure 12

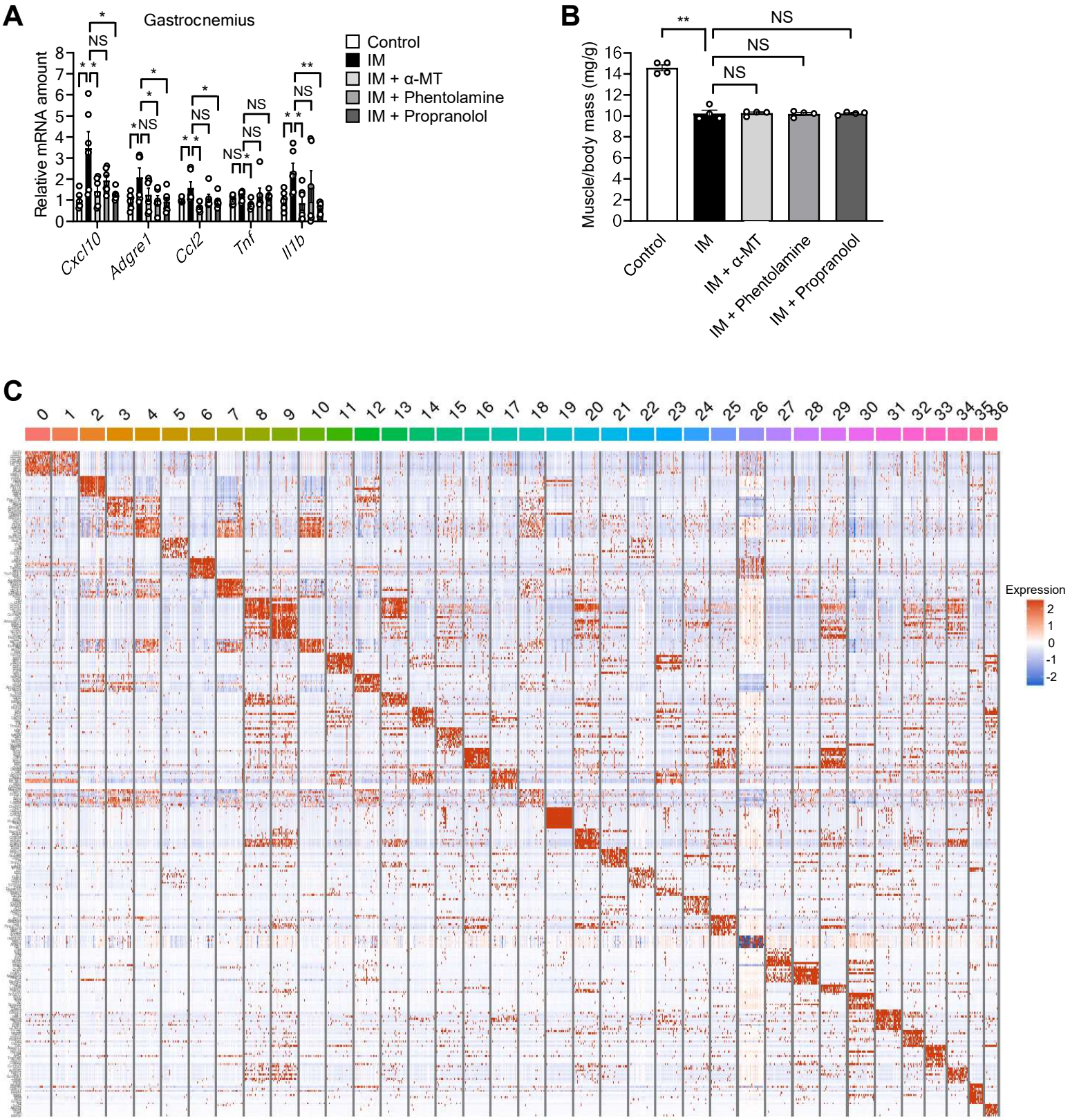

Figure S12, related to Figure 6. Sympathetic nerve activation contributes to muscle inflammation induced by limb immobilization

(A and B) RT-qPCR analysis of inflammation-related gene expression in gastrocnemius (n = 6 mice) (A) as well as the ratio of gastrocnemius muscle mass to body mass (n = 4 mice) (B) for mice subjected to intraperitoneal injection of α-MT, phentolamine, propranolol, or vehicle daily for 10 days with or without concomitant cast-immobilization. Data are means ± SEM. *$p < 0.05$, **$p < 0.01$, NS (two-way ANOVA with the Bonferroni post hoc test).

(C) Heat map for the expression of all genes in the cell clusters of the colon identified by scRNA-seq analysis.

Supplemental Figure 13

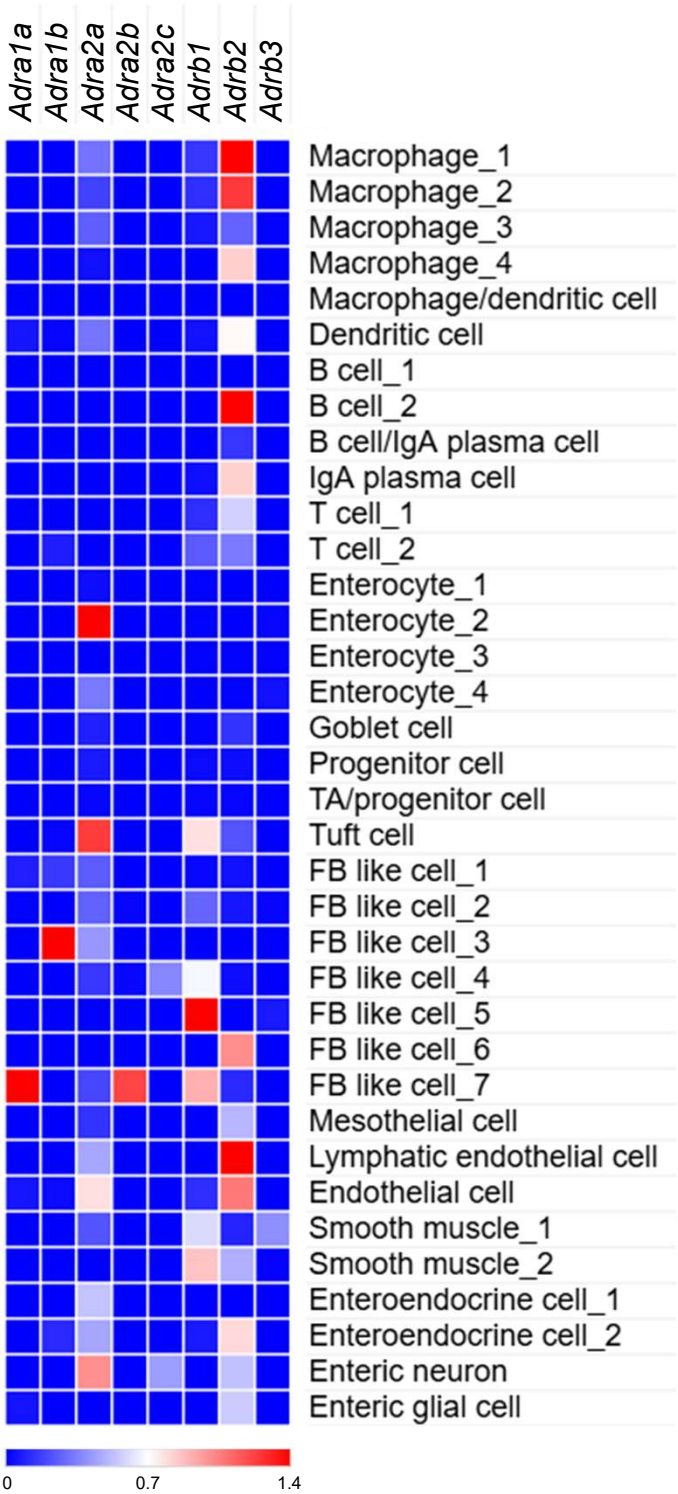

Figure S13, related to Figure 6. Heat map for expression of adrenergic receptor genes in cell clusters of the colon as determined by scRNA-seq analysis

Supplemental Figure 14

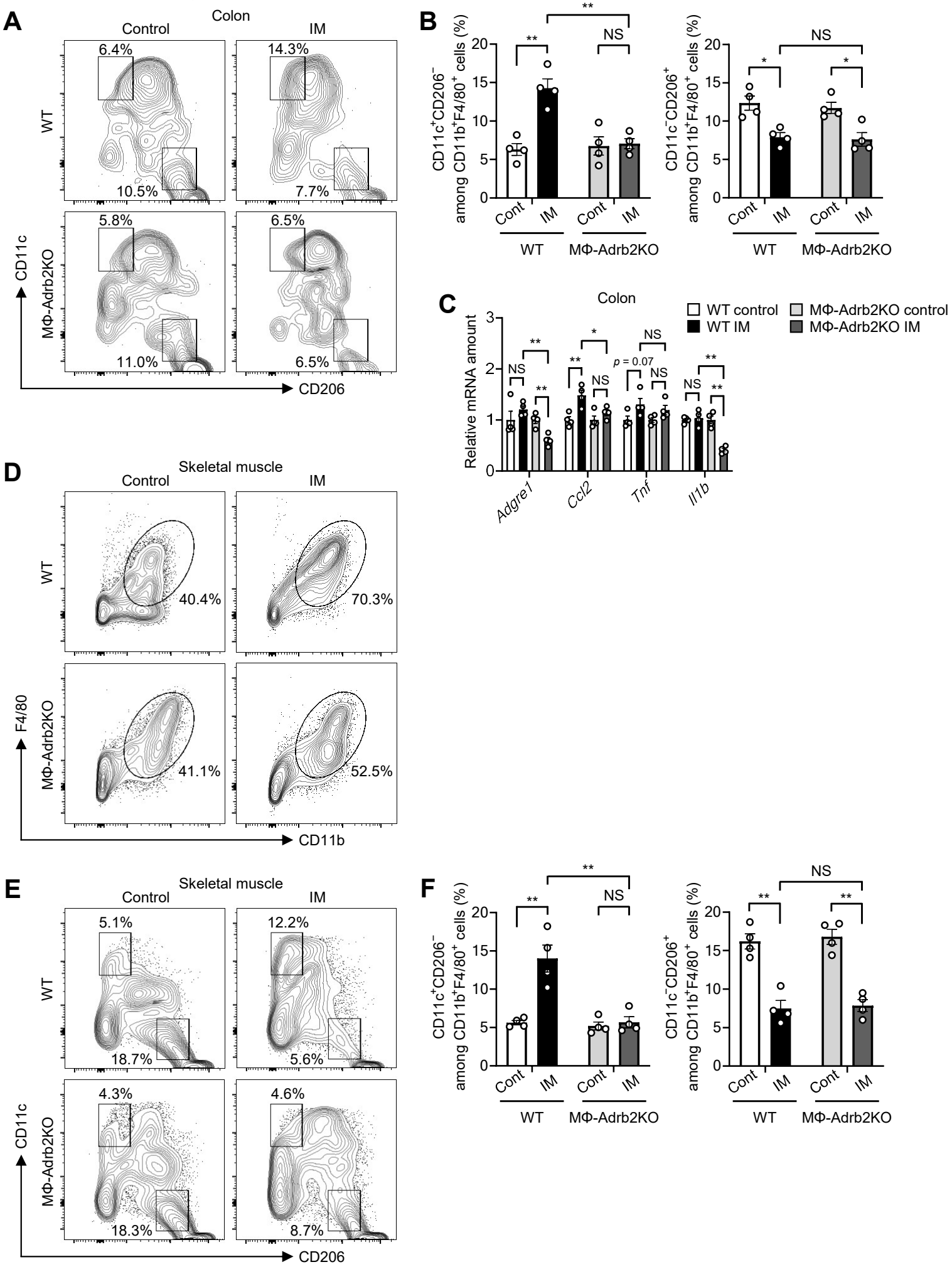

Figure S14, related to Figure 7. Intestinal and muscle inflammation induced by prolonged limb immobilization is attenuated in MΦ-Adrb2KO mice

(A–C) Representative flow cytometric analysis (A) and the percentage (B) of $CD11c^{+}CD206^{-}$ cells or $CD11c^{-}CD206^{+}$ cells among $CD11b^{+}F4/80^{+}$ cells as well as RT-qPCR analysis of inflammation-related gene expression (C) in the colon of WT or MΦ-Adrb2KO mice subjected (or not) to cast-immobilization for 10 days (n = 4 mice).

(D–F) Representative flow cytometric analysis of $CD11b^{+}F4/80^{+}$ cells among $CD45^{+}Ly6G^{-}$ cells (D) as well as representative flow cytometric analysis (E) and the percentage (F) of $CD11c^{+}CD206^{-}$ cells or $CD11c^{-}CD206^{+}$ cells among $CD11b^{+}F4/80^{+}$ cells in hind limb skeletal muscle of WT or MΦ-Adrb2KO mice subjected (or not) to cast immobilization for 10 days (n = 4 mice).

All quantitative data are means ± SEM. *$p < 0.05$, **$p < 0.01$, NS (two-way ANOVA with the Bonferroni post hoc test).

Supplemental Figure 15

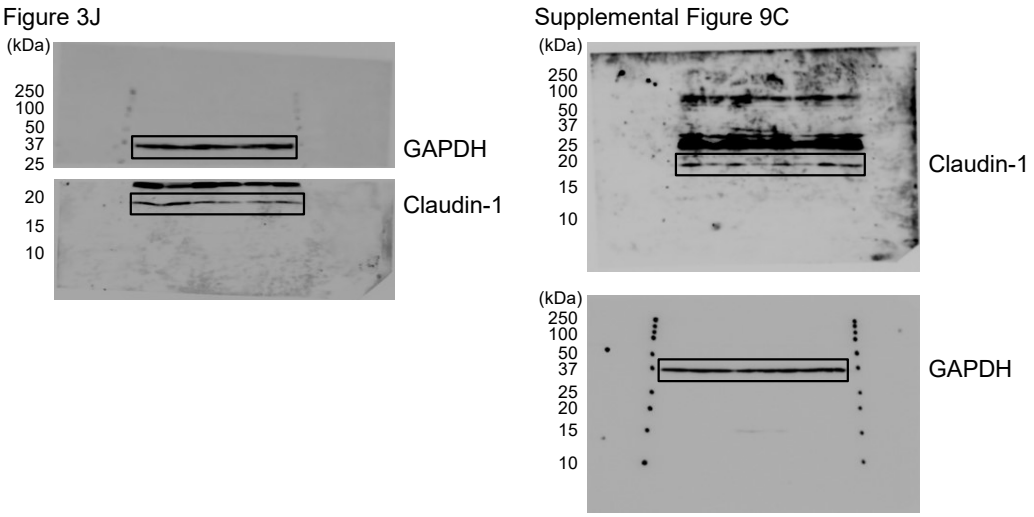

Figure S15, related to Figures 3 and S9. Uncropped immunoblot images
Black boxes contain the areas shown in the indicated figures.

Supplemental Table 1

Cluster	Key genes
Macrophage_1	*Cd68, Mrc1, Ctsa, Cd163*
Macrophage_2	*Itgam, Fcer1g, Mrc1, Retnla*
Macrophage_3	*Cd68, Fcer1g, Apoe, C1qb*
Macrophage_4	*Cd14, Itgam, Marco, Saa3*
Macrophage/dendritic cell	*Cd80, Cd86, Apol7c, Cacnb3*
Dendritic cell	*Itgax, Cd209a, Clec9a, Cst3*
B cell_1	*Cd19, Cd79a, Ighd, Ighm*
B cell_2	*Cd19, Cd79a, Ighd, Ighm*
B cell/IgA plasma cell	*Igha, Mzb1, Cd19*
IgA plasma cell	*Igha, Mzb1, Jchain*
T cell_1	*Cd3d, Cd8a, Cd4, Trac*
T cell_2	*Trbc1, Cd4, Id2, Il2ra*
Enterocyte_1	*Slc26a2, Aqp8, Slc20a1, Tgm3*
Enterocyte_2	*Slc26a2, Aqp8, Guca2a, Cyp2c55*
Enterocyte_3	*Slc26a2, Aqp8, Saa1, Car4*
Enterocyte_4	*Slc26a2, Slc26a3, Stard10, Fth1*
Goblet cell	*Tff3, Fcgbp, Clca1*
Progenitor cell	*Sox9, Cdk6, Muc4, Agr2*
TA/progenitor cell	*Ube2c, Sox9, Pigr, Ppp1r1b*
Tuft cell	*Trpm5, Pou2f3, Sh2d6*
FB like cell_1	*Col1a1, Fn1, Gsn, Dpt*
FB like cell_2	*Col1a1, Fn1, Ccn2, Adamdec1*
FB like cell_3	*Col1a1, Fn1, Pi16, Inmt*
FB like cell_4	*Col1a1, Fn1, Tnc, Sema3f*
FB like cell_5	*Fn1, Col1a2, Kit, Ano1*
FB like cell_6	*Col1a1, Col1a2, Clu, Mfge8*
FB like cell_7	*Col1a1, Col1a2, Jam2, Angptl2*
Mesothelial cell	*Msln, Wt1, C3, Slpi*
Lymphatic endothelial cell	*Lyve1, Pecam1, Ccl21a, Mmrn1*
Endothelial cell	*Pecam1, Vwf, Flt1, Egfl7*
Smooth muscle_1	*Des, Actg2, Acta2, Myh11*
Smooth muscle_2	*Actg2, Acta2, Hhip, Myh11*
Enteroendocrine cell_1	*Chga, Gcg, Pyy, Ins1*
Enteroendocrine cell_2	*Chga, Piezo2, Neurod1, Tph1*
Exocrine cell	*Ctrb1, Cela2a, Cela3b, Cpa1*
Enteric neuron	*Ncam1, L1cam, Tac1, Vip*
Enteric glial cell	*Gfap, Ncam1, L1cam, Adam11*

Table S1, related to Figures 6 and 7. Genes that characterize cell clusters of the colon identified by scRNA-seq analysis of control mice and mice subjected to cast-immobilization for 10 days

The exocrine cell cluster is characterized by expression of genes for digestive enzymes including *Ctrb1*, *Cela2a*, *Cela3b*, and *Cap1*, all of which are commonly expressed in pancreatic exocrine cells. Moreover, this cluster was detected in a specific sample. Given that this cluster may have been derived from ectopic pancreatic tissue congenitally admixed with intestinal tissue, or from contaminating pancreatic tissue artefactually introduced during intestinal tissue collection, it was excluded from further analysis.

Supplemental Table 2

Mouse gene	Primers (5' → 3')
36b4	FWD: GAGGAATCAGATGAGGATATGGGA
	REV: AAGCAGGCTGACTTGGTTGC
Adgre1	FWD: TGCCTCCCTGACTTTCAAAT
	REV: TGGCATTGCTGTATCTGCTC
Alt2	FWD: CAGACCCAGACAACATTTACCTG
	REV: CGCGGAGTACAAGGGATACTG
Bnip3	FWD: TTCCACTAGCACCTTCTGATGA
	REV: GAACACCGCATTTACAGAACAA
Ccl2	FWD: AGGTGTCCCAAAGAAGCTGTA
	REV: ATGTCTGGACCCATTCCTTCT
Cxcl10	FWD: TCCCTCTCGCAAGGAC
	REV: TTGGCTAAACGCTTTCAT
Fbxo32	FWD: GCAAACACTGCCACATTCTCTC
	REV: CTTGAGGGGAAAGTGAGACG
Foxo3a	FWD: CAGGCTCCTCACTGTATTCAGCTA
	REV: CATTGAACATGTCCAGGTCCAA
Il1b	FWD: GCTGAAAGCTCTCCACCTCA
	REV: AGGCCACAGGTATTTTGTCG
Klf15	FWD: ACCGAAATGCTCAGTGGGTTACCTA
	REV: GGAACAGAAGGCTTGCGAGTCA
Myh4	FWD: GAGCTACTGGATGCCAGTGAGCGC
	REV: CTGGACGATGTCTTCCATCTCTCC
Ptprc	FWD: ATGGTCCTCTGAATAAAGCCCA
	REV: TCAGCACTATTGGTAGGCTCC
Tnf	FWD: CATCTTCTCAAAATTCGAGTGACAA
	REV: TGGGAGTAGACAAGGTACAACCC
Trim63	FWD: GCTGGTGGAAAACATCATTGACAT
	REV: CATCGGGTGGCTGCCTTT

Table S2, related to STAR METHODS. Sequences of mouse primers for RT-qPCR analysis
FWD, forward; REV, reverse.

Supplemental Table 3

Human gene	Primers (5’ → 3’)
36B4	FWD: TTGTGGGAGCAGACAATGTG
	REV: TATTGGCCAGCAACATGTCC
ADGRE1	FWD: CCAGTGTTAATGCCGAAGTCT
	REV: GTGAACAGGTAAGCCATGACA
CCL2	FWD: CAGCCAGATGCAATCAATGCC
	REV: TGGAATCCTGAACCCACTTCT
CXCL10	FWD: TGCCATTCTGATTTGCTGCC
	REV: TGCAGGTACAGCGTACAGTT
IL1B	FWD: TTCGACACATGGGATAACGAGG
	REV: TTTTTGCTGTGAGTCCCGGAG
TNF	FWD: GAGGCCAAGCCCTGGTATG
	REV: CGGGCCGATTGATCTCAGC

Table S3, related to STAR METHODS. Sequences of human primers for RT-qPCR analysis
FWD, forward; REV, reverse.